Small-angle scattering techniques for peptide and peptide hybrid nanostructures and peptide-based biomaterials

Advances in Colloid and Interface Science 318 (2023) 102959

Contents lists available at ScienceDirect

Advances in Colloid and Interface Science

journal homepage: www.elsevier.com/locate/cis

Historical Perspective

Small-angle scattering techniques for peptide and peptide hybrid nanostructures and peptide-based biomaterials

Ian W. Hamley *, Valeria Castelletto

Department of Chemistry, University of Reading, Whiteknights, Reading RG6 6AD, UK

ARTICLE INFO

Keywords:
Small-angle scattering
Peptides
Nanostructures
Biomaterials
SAXS
SANS

ABSTRACT

The use of small-angle scattering (SAS) in the study of the self-assembly of peptides and peptide conjugates (lipopeptides, polymer-peptide conjugates and others) is reviewed, highlighting selected research that illustrates different methods and analysis techniques. Both small-angle x-ray scattering (SAXS) and small-angle neutron scattering (SANS) are considered along with examples that exploit their unique capabilities. For SAXS, this includes the ability to perform rapid measurements enabling high throughput or fast kinetic studies and measurements under dilute conditions. For SANS, contrast variation using H_2O/D_2O mixtures enables the study of peptides interacting with lipids and TR-SANS (time-resolved SANS) studies of exchange kinetics and/or peptide-induced structural changes. Examples are provided of studies measuring form factors of different self-assembled structures (micelles, fibrils, nanotapes, nanotubes etc) as well as structure factors from ordered phases (lyotropic mesophases), peptide gels and hybrid materials such as membranes formed by mixing peptides with polysaccharides or peptide/liposome mixtures. SAXS/WAXS (WAXS: wide-angle x-ray scattering) on peptides and peptide hybrids is also discussed, and the review concludes with a perspective on potential future directions for research in the field.

1. Introduction

1.1. Peptide nanostructures and peptide-based biomaterials

Appropriate design of peptide sequences including hydrophobic and hydrophilic domains can lead to self-assembly of peptides or peptide hybrids such as conjugates of peptides with lipids, polymers or polysaccharides. Self-assembly (and/or aggregation) of peptides and peptide hybrids has been extensively reviewed [1–14]. The incorporation of peptides within biomaterials endows them with the diversity of functionalities of peptides, for example recognition or binding of specific sequences by target molecules or catalytic activity. Examples include peptide-functionalized gels for applications in cell culture and tissue engineering or peptide-based biomaterials with activity in catalysis or analyte detection, or in the delivery of therapeutics. Other examples rely on the aggregation of amyloid peptides based on the unique materials properties of peptide β-sheet fibril structures, of which examples can be found in nature as well as designed materials. There are many reviews that cover peptide biomaterials, examples include references [15–32]. Here, the use of small-angle scattering to probe self-assembling peptide-based molecules and materials is discussed. SAXS and SANS measurements on peptide nanostructures that result from self-assembly in solution are considered. In addition, SAS data from peptide gels and mixtures with polysaccharides or lipids are discussed, along with SAXS/WAXS studies on hierarchically ordered peptide-based systems and materials.

1.2. Small-angle scattering

Small-angle scattering is a powerful method to probe the structure of peptides and peptide-based biomaterials in situ. This valuable tool, in our work and that of many other researchers, is often complemented with real-space imaging of nanostructures using microscopy methods including electron microscopy or atomic force microscopy (AFM) along with optical microscopy for larger structures or liquid crystal texture analysis etc.

Given that this Special Issue is aimed at small-angle scattering specialists, we do not provide an overview of the technique itself here. Anyway, further information on the technique is available in many books [33–40] and reviews [41–55]. The method provides information

* Corresponding author.
E-mail address: I.W.Hamley@reading.ac.uk (I.W. Hamley).

https://doi.org/10.1016/j.cis.2023.102959
Received in revised form 3 July 2023;
Available online 7 July 2023

on mesoscopic or nanoscale structure in the system (typically on a 5–50 nm length scale) based on analysis of the scattered intensity as a function of wavevector $q = 4\pi\sin\theta/\lambda$ where 2θ is the scattering angle and λ is the wavelength. In the following, we consider both form factor scattering from nanostructure shape and size (intra-particle scattering) as well as structure factor (inter-particle scattering) effects for peptide-based assemblies and materials.

X-rays are scattered by electrons, so small-angle x-ray scattering depends on electron density variations in a system. In contrast, neutrons are scattered by nuclei and SANS depends on the scattering length density profile (this depends on the nuclear scattering factors). Lab-based instruments are available for SAXS (or SAXS/WAXS) or there are synchrotron sources of x-rays including SAXS (or SAXS/WAXS) beamlines at synchrotron facilities around the world [39]. SANS may be performed at central facilities, with a nuclear reactor source of neutrons or a spallation source. Again, facilities are located around the globe [39]. Many SANS instruments enable short camera lengths covering a wide-angle range (i.e. WANS, although this term is not used in the field) and there is also the possibility to perform neutron fibre diffraction. SAXS benefits from the ability to do laboratory measurements or from the availability of high flux synchrotron instruments, enabling rapid measurements (including fast time-resolved experiments) as well as experiments on dilute solutions with weak scattering features. A major advantage of SANS is the ability to perform contrast variation measurements using mixtures of deuterated and protonated molecules. SANS also enables longer measurements without the risk of beam damage of samples (leading to ionisation and molecular dis-assembly) which can occur with synchrotron SAXS [39].

Previous reviews of SAS on peptide assemblies and biomaterials are available [56,57].

In this Review, we first discuss small-angle scattering measurements from peptide and peptide conjugates in solution using SAXS and SANS. Most measurements are for aqueous solutions and involve analysis of the form factor, which is obtained in sufficiently dilute solution, for which structure factor effects are negligible. We then describe structure factor effects, exemplified in a range of peptide-based systems including gels, lyotropic mesophases or mixtures with lipid vesicles etc. Then *ab initio* methods to model SAS data for peptides are outlined, in particular BioSAXS data, using techniques typically used for proteins, including analysis of the pair distance distribution function, shape reconstruction, bead models, atomistic models and others.

We also discuss anisotropic SAS data obtained from self-assembled peptide solutions that show flow alignment such as dispersions of amyloid peptide fibrils or peptide nanotubes, or from other aligned peptide biomaterials such as hybrid membranes. We finally provide examples of SAXS/WAXS studies on peptide assemblies and peptide-based biomaterials, which have a degree of local order (i.e. on the length scale of ca. 1–10 Å) which can be probed by WAXS. This is exhibited by assemblies with ordered secondary structure (such as α-helix or β-sheet) and in systems such as peptide gels or hybrid biomaterials such as peptide/saccharide mixtures, as well as polymer/peptide conjugates with hierarchical order due, for example, to polymer crystallization.

This review is intended to outline key concepts via examples from selected studies that highlight the state-of-the-art in the use of SAS to study peptide-based systems. SAXS and SANS are powerful and widely-used methods, and it is not possible to review every example of their application to study peptide structures. We apologise for any egregious omissions.

2. Solution SAXS and SANS

2.1. Form factors

The SAXS form factor from unaggregated peptide can readily be distinguished from that of peptide assemblies, as shown through the examples presented in Fig. 1. Fig. 1b shows the shape of a monomer form

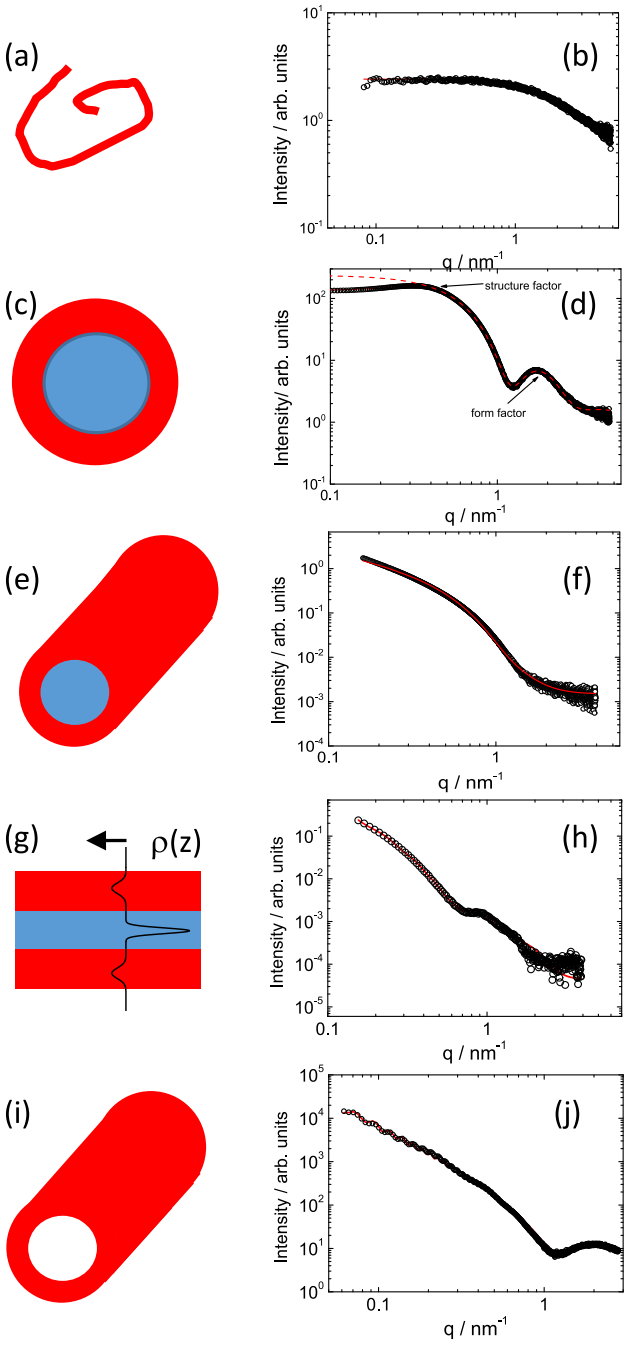

Fig. 1. Examples of form factor fits to SAXS data from our work on surfactant-like peptides and lipopeptides: (a) Gaussian coil representing a monomeric peptide, (b) SAXS data for a 1 wt% aqueous solution of P_6E (open symbols) with fit to Gaussian coil form factor (red line) [58]. (c) Sketch of core-shell spherical micelle, (d) SAXS data from a 1 wt% solution of lipopeptide C_{16}-CSK_4RGDS with fit to core-shell micelle form factor (dashed red line) and also allowing for structure factor (solid red line) (e) Schematic of core-shell cylinder, (f) SAXS data for a 1 wt% aqueous solution of A_6R (open symbols) with fit to core-shell cylinder form factor (red line) [59]. (g) Schematic of a bilayer with superposed electron density profile represented by bilayer Gaussian model (three Gaussian representation), with large dip in the lipid interior (blue lamella) and positive relative electron density in the peptide headgroup regions (red domains), (h) SAXS data for an 0.5 wt% aqueous solution of lipopeptide C_{16}-YEALRVANEVTLN (open symbols) with Gaussian bilayer form factor fit [60]. (i) Schematic of a nanotube, (j) SAXS data for an 1 wt% aqueous solution of lipopeptide C_{16}-KKFFVLK (open symbols) with nanotube (i.e. hollow cylindrical shell) + Gaussian bilayer (to account for electron density cross-section across the nanotube wall) form factor fit [61]. Reproduced from ref. [62].

factor, which has been fitted with a Gaussian coil (Fig. 1a) model to represent the unordered conformation [39]. It has a characteristic flat shape at low q, curving over at high q. The shape of this form factor can be contrasted from those of the assembled structures shown in the other parts of Fig. 1.

SAXS data from a lipopeptide or peptide micelle can often been fitted using a core-shell (two electron density level) sphere (Fig. 1c) form factor [63–69], an example being shown in Fig. 1d. This figure also shows the influence of the structure factor (solid red line model fit) which leads to a broad peak at low q. For the spherical micelle case, the structure factor may be the simple hard-sphere structure factor model as in the fit in Fig. 1d.

SAXS can be used to probe the evolution of peptide nanostructures such as spherical micelles in response to triggers such as enzymatic cleavage. Addition of α-chymotrypsin to a conjugate of βAβAKLVFF (βA: β^2-alanine) and PEG300 leads to cleavage of the F-F bond and the initial spherical micelle structure is disrupted and instead monomers of βAβAKLVF peptide are produced, as shown by SAXS form factor analysis [70]. Remarkably, addition of one extra terminal F in βAβAKLVFF leads to fibril formation, the SAXS data being fitted with a core-shell cylinder form factor. In a related vein, SAXS form factor data (with cryo-TEM images) shows that C_{16}-KKFFVLK forms nanotubes and helical ribbons at room temperature but cleavage using α-chymotrypsin releases lipopeptides C_{16}-KKF and C_{16}-KKFF which instead self-assemble into 5–6 nm diameter spherical micelles, while the other released products, peptides FVLK and VLK, do not adopt well-defined aggregate structures [63]. In another example, SAXS (and TEM) data for a C_{16} lipopeptide bearing a cell-penetrating peptide sequence as well as an matrix metalloprotease (MMP-2) substrate sequence shows a transition from core-shell cylindrical micelles to spherical micelles after enzymatic cleavage [71].

For fibrils (Fig. 1e) formed by peptides (in particular those with a β-sheet conformation) or conjugates such as lipopeptides, a uniform [41] or core-shell [72] cylinder form factor can be used to fit SAXS or SANS data. A representative fit is shown in Fig. 1f. A core-shell model is generally required since there is usually a contrast difference between the core of the peptide fibril and the exterior. This is evident for instance in the case of PEG-peptides with a PEG corona [72,73]. However, SANS data for Aβ(10–35)-PEG (conjugate with PEG3000) and the Amyloid β(10–35) peptide alone was analysed (at different pH values) considering a simple homogeneous cylindrical structure [74]. Modified Guinier plots (analysis of $\ln[qI(q)]$ vs. q^2) were used to obtain the cylinder radius, and the intercept $I(0)$ of such plots gives the mass per unit length provided the data are obtained on an absolute scale [74].

Contrast variation SANS using selectively deuterated molecules is a powerful tool to elucidate the structure of core-shell structures and has been used to probe the structure of core-shell cylinders formed by the conjugate 2-Nap-FF (Nap: naphthyl) [75], using the undeuterated parent compound and a series of partly deuterated derivatives with either the naphthyl ring deuterated (termed 2dNapFF) or either or both of the phenylalanine residues in 2NapdF, 2NapFdF or 2NapdFdF. Fig. 2 shows SANS data obtained in D_2O for these derivatives. The notable differences in form factor can be fitted corresponding to different shell thicknesses (shown schematically above the SANS intensity profiles) in a core-shell cylinder form factor model.

For nanotapes (observed for lipopeptides for example), a form factor

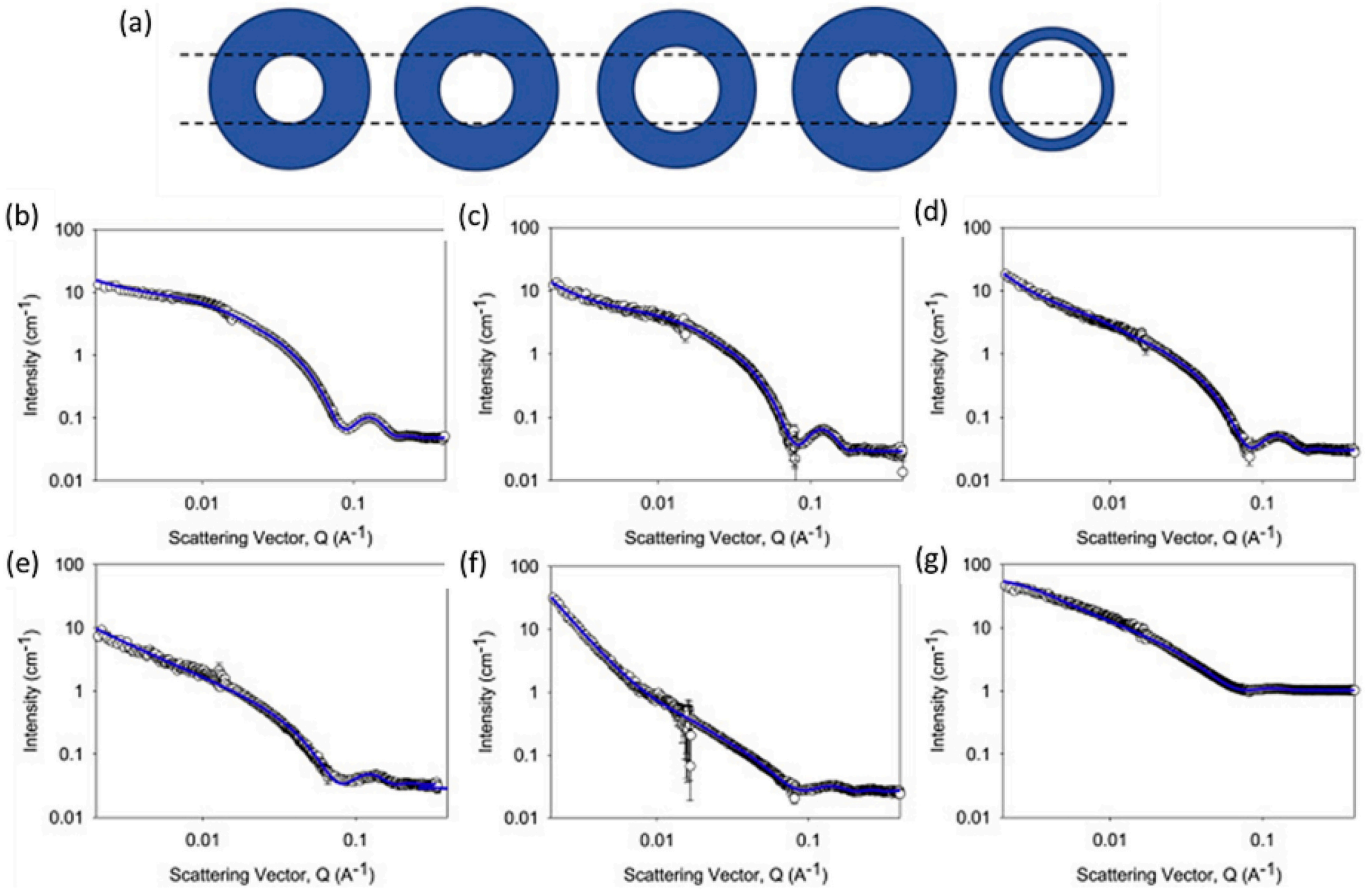

Fig. 2. Contrast-variation SANS data from a series of partially deuterated derivatives of 2-Nap-FF (2-naphthyl-diphenylalanine). (a) Schematic of hollow cylinder structures obtained from form factor fitting of the SANS data for 2NapFF, 2dNapFF, 2NaphFdF, 2NapdFhF, and 2NapdFdF in D_2O from the fits to the SANS data in (b)–(g). (b–g) SANS data (open circles) and fits (blue lines): (b) 2NapFF in D_2O, (c) 2dNapFF in D_2O, (d) 2NaphFdF in D_2O, (e) 2NapdFhF in D_2O, (f) 2NapdFdF in D_2O, (g) 2NapdFdF in H_2O. From reference [75].

developed for lipid bilayers can successfully be used to fit data. This so-called Gaussian bilayer form factor comprises three Gaussian functions, one of which represents the electron density (in the case of SAXS) of the lipid-chain rich core (negative amplitude), the other two being (positive amplitude) Gaussians representing the electron density of the charged head-groups (Fig. 1g). The form factor equations and definitions can be found in the original paper where this form factor was reported [76], and are used in many papers from our group [77–83], an example of data fitted to such a model is shown in Fig. 1h. Other approaches have been used to fit form factors for solutions containing lipopeptide nanotape assemblies such as the use of a core-shell parallelepiped form factor [84].

Peptide β-sheets may twist to form twisted tapes or helical nanoribbon structures. The latter may be considered to be "unwound" peptide nanotubes, indeed in some systems twisted nanoribbons and closed nanotubes coexist. SAXS from helical ribbon peptide structures may be fitted using form factors available in the literature [85–89]. A form factor for twisted ribbons has been derived and applied to fit SAXS data obtained from solutions of C_{16}-K [89]. The self-assembly of other C_n-K lipopeptides with n = 12, 14, 16 was also studied (including different enantiomers of C_{16}-K) and the nanostructure was also examined for a given lipopeptide as a function of pH and salt concentration. Fig. 3 shows helical ribbons formed by C_{16}-K (AFM image) along with fitted SAXS data at several pH values and a schematic of a ribbon showing the parameters for the form factor [89].

The assembly of different types of peptides into several classes of nanotubes (Fig. 1i) has also been observed, and data have been fitted with corresponding form factors (e.g. Fig. 1j) [78,90,91]. A simple form factor is available for nanotubes in the case of long fibrils with a thin wall [92]. This expression has been used to fit SAXS data from aqueous solutions of the surfactant-like peptide A_6K, and is able to reproduce the periodicity of the form factor oscillations that arise from the nanotube diameter, even at higher concentration where a nematic phase of nanotubes is reported [92]. Longer alanine-sequence homologues A_8K and $A_{10}K$ form ribbon structures, the SAXS data being fitted using elliptical cylinder form factors [93]. Another approximation applies if the nanotube radius $R >> t$, where t is the tube wall thickness (e.g. of a bilayer), then the high q part of the small-angle scattering data results from the structure of the tube wall, which can be described using models such as the Gaussian bilayer form factor [61].

The cyclic octapeptide Lanreotide (a therapeutic peptide hormone inhibitor) forms nanotubes for which SAXS shows a well-defined radius and wall thickness (Fig. 4) [94]. Modelling of the molecular packing constrained by the wall thickness and spacings from fiber diffraction leads to the model shown in Fig. 4 with peptides tilted with respect to the nanotube axis. The peptide nanotubes form a hexagonal phase in aqueous solution at concentrations 14 wt% and above, as revealed by structure factor peaks in the low q SAXS data [94,95]. SAXS also shows heating-induced dissociation of the β-sheet-based nanotubes [95]. The (re-)association involves intermediate species including dimers and helical ribbons which finally close into tubes, as eludicated in a detailed study using SAXS and electron microscopy [96]. The packing of the molecules in the nanotube walls is stabilized by close contacts between D-Nap (2-D-naphthylalanine) and D-Trp residues and a study using a library of non-natural (and natural) aromatic D-amino acids variants of these showed, via SAXS, a large difference in nanotube diameter (4-fold

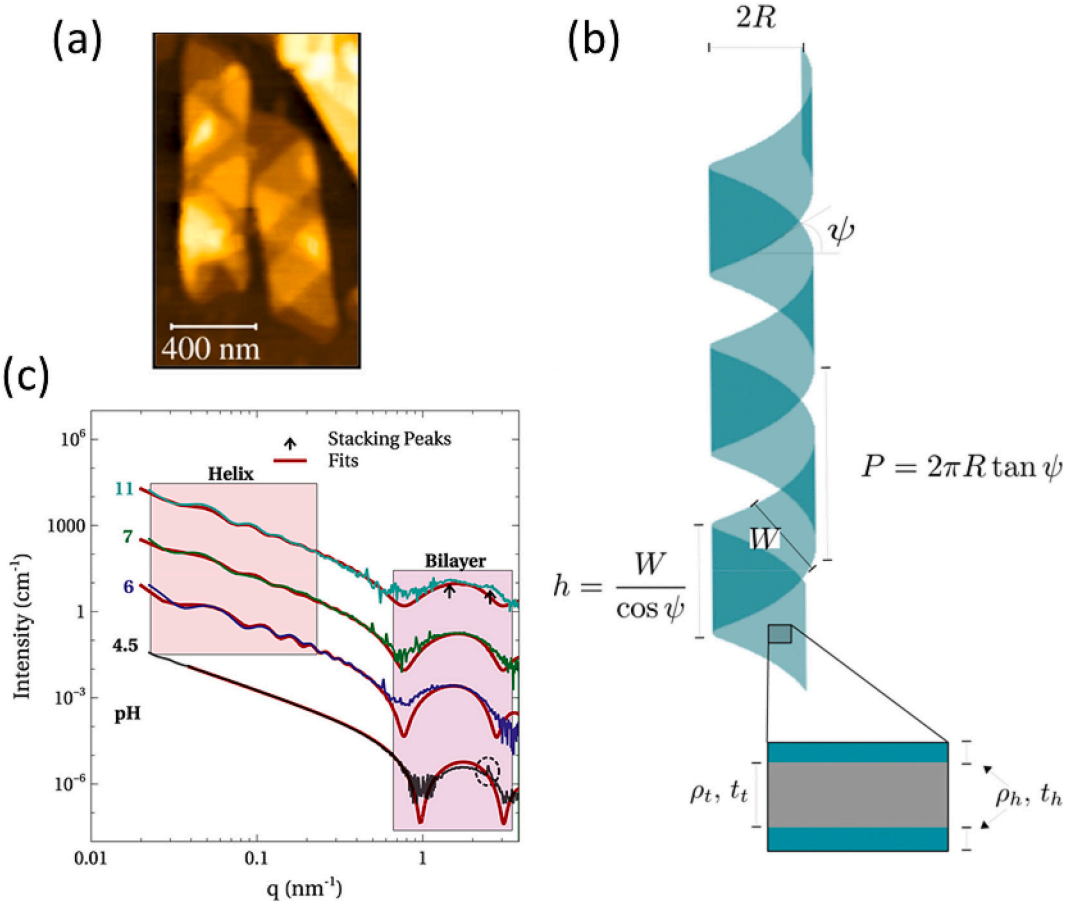

Fig. 3. Helical ribbons formed by lipopeptides. (a) AFM image of C_{16}-K at pH ~ 8.5, (b) Parameterization of form factor for helical ribbons, R denotes radius, ψ the twist angle, P the pitch, h and W the tape and membrane width, ρ_t and ρ_h are electron densities and t_t, t_h are thicknesses of tape layers (subscript t indicates hydrophobic tail and h denotes headgroup), (c) SAXS data for C_{16}-K at pH values shown (coloured lines) along with form factor fits (red lines, based on a planar bilayer for pH = 4.5 data or helix for pH = 6, 7, 11 form factors). Observed peaks are shown by arrows or dotted circle. From reference [89].

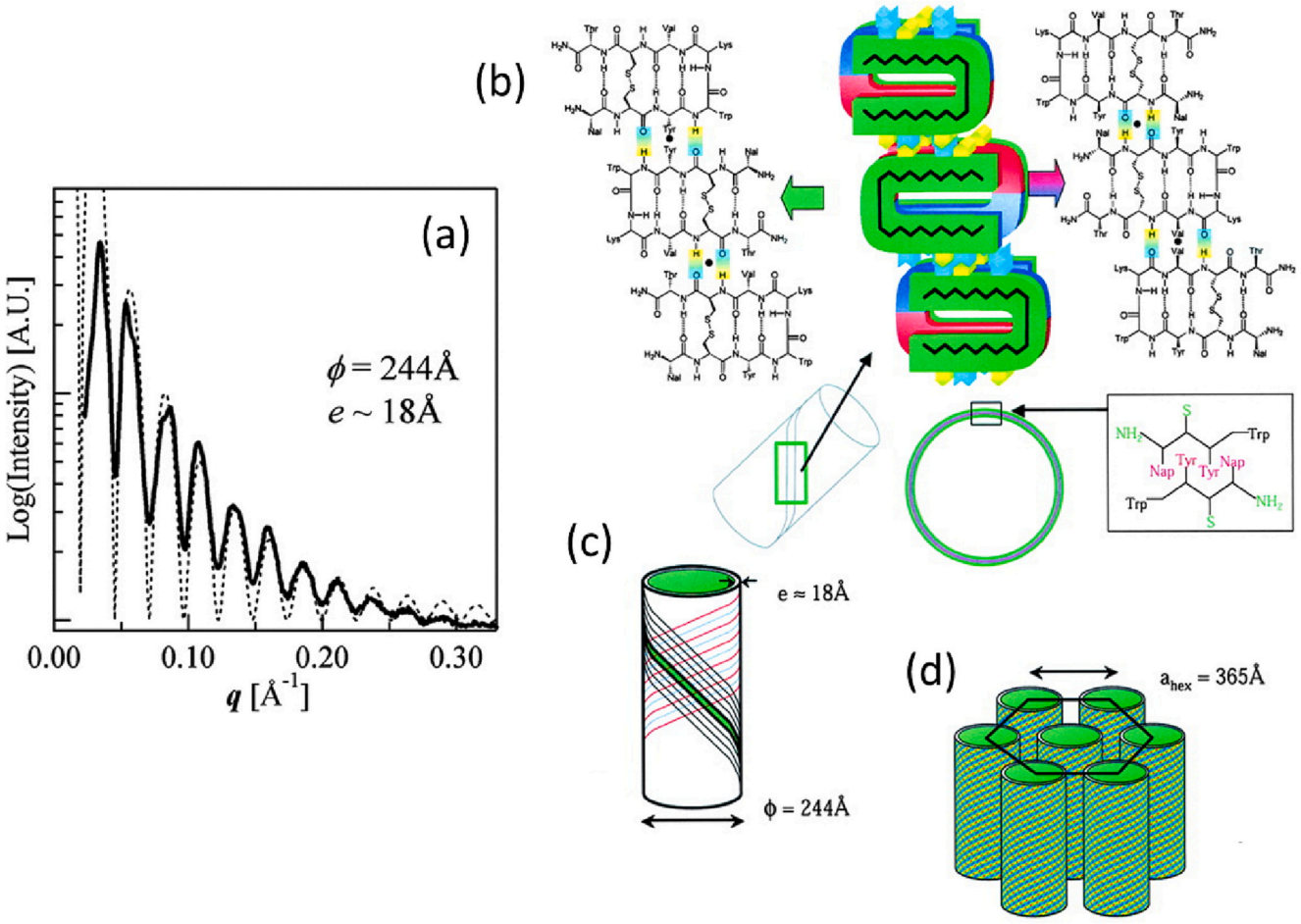

Fig. 4. SAXS data and model for nanotube structure for cyclic octapeptide Lanreotide. (a) SAXS data from 14 wt% aqueous solution with nanotube diameter ϕ and wall thickness e indicated (b,c) Model for nanotube packing, hydrogen bond donors and acceptors indicated in yellow and blue respectively, selected residues interdigitating are shown (Nap = 2-D-naphthylalanine, Trp = D-tryptophan), (d) Packing of nanotubes in hexagonal phase with lattice parameter shown. From reference [94].

variation) [97]. The nanotube diameter can also be tuned by choice of counterion [98,99]. The mineralization of Lanreotide gels in the presence of silica was also monitored by time-resolved SAXS and electron microscopy which revealed the silica nanotube structure [100].

Reversible thermal dissociation of nanotubes was also observed in SAXS studies of the lipopeptide C_{16}-KKFFVLK which contains the (inverse) KLVFF sequence Aβ16–20 [63,61]. SANS measurements along with complementary SAXS provides data under two contrast conditions, as observed for example for nanotubes of the Aβ16–22 peptide KLVFFAE at pH 2 in mixed solvent (acetonitrile/D_2O) [90]. As well as thermal transitions, nanotube structures can be controlled via choice of solvent, for example SANS on solutions of peptide KI_4K showed a transition from nanotubes to helical/twisted ribbons and then to thin fibrils with addition of acetonitrile [101]. This was ascribed to the reduced hydrophobic interactions and the consequent weakening of the lateral stacking between the β-sheets. Other work on peptide nanotubes that includes SAXS studies has been reviewed [9,102].

Irregular peptide assemblies have been observed for systems such as bola-amphiphilic or 'blocky' peptides. The SAXS data for R_4F_4 has been fitted using a combination of mass fractal form factors and long cylindrical shell form factors, whereas the bola-amphiphile homologue $R_2F_4R_2$ has nanotape form factor features [103]. A mass fractal model was also used to fit SAXS data for $[RF]_4$ and was combined with a long cylindrical shell form factor to model data from mixtures with $P[RF]_4$ [104]. SAXS data for the Penetratin cationic cell-penetrating peptide was fitted using a combination of a Fisher-Burford fractal form factor [39,105] to describe the low q part and a generalized Gaussian coil function for the high q part [106]. Addition of (200 base pair calf thymus) DNA led to the development of a Bragg peak due to the formation of ordered complexes with the peptide. SAXS and SANS data for peptides from the $[RF]_n$ (n = 1–5) series were fitted using a fractal model to describe the low q power law intensity decay [107]. based on a fractal form factor with exponential cut-off due to Teixeira [108] along with other components to describe the high q scattering or a cylinder form factor for $[RF]_4$ or $[RF]_5$. The form factor developed by Beaucage to describe fractal objects with multi-level structure [39,109,110] was used to fit SAXS data for the $[EF]_4$ analogue containing anionic glutamic acid in the alternating peptide oligomer sequence [111]. A heptapeptide KIWFQNR derived from Penetratin forms irregular fractal-like structures for which the SAXS data could be described by a low q power law and a high q Gaussian coil form factor for the local structure [112]. In contrast, a cylindrical core- shell form factor is observed when DNA is added, which leads to fibril formation.

Although there are many examples of SANS studies of self-assembled peptides in D_2O or H_2O/D_2O mixtures, contrast variation SANS using selectively labelled peptides has very rarely been employed in the measurement of peptide form factors (actually we surprisingly could not find any examples in a literature search), although it has been used in a few studies (as mentioned above) on peptide conjugates [75] or for self-assembled polymer-peptide conjugates using deuterated polymers [113,114]. Contrast variation SANS using mixtures of protonated and deuterated lipids has been used to probe interactions of peptides with

lipid membranes as described in the following Section. This is presumably in part due to the commercial availability of deuterated lipids or monomers, whereas deuteration of peptides requires custom synthesis, with the added cost of deuterated amino acids. Peptides can be synthesized using established methods (solid phase synthesis) using deuterated monomers, or via recombinant methods, with the expression system acting in media containing deuterated amino acids. Further information on deuteration methods for peptides is available elsewhere [115].

SAXS has played an essential role in elucidating changes in the nanostructure of peptide conjugates upon changing the number or length of lipid chains. For example, lipopeptides with the Toll-like receptor agonist hexapeptide CSK_4 and bearing one, two or three hexadecyl (C_{16}, palmitoyl) lipid chains form distinct nanostructures, predominantly micelles for the variants with one and two lipid chains but nanotapes (coexisting with globules) for the three lipid chain analogue [66]. This was confirmed by SAXS form factor analysis as well as cryo-TEM images. Lipopeptides bearing the bioactive RGDS sequence attached via a GGG or WGG linker to C_{14} or C_{16} lipid chains also show different nanostructures, the C_{14}-WGGRGDS lipopeptide in particular shows a nanotube form factor in contrast to the others which show nanotape form factor features [83]. The two tryptophan-containing peptides also show oriented SAXS patterns from a flow-aligning nematic phase. SAXS shows notable differences in the form factor of solutions of lipopeptides PRWG-C_{18} and PRWG-$(C_{18})_2$ the first showing features of the form factor of cylinders including a low q intensity scaling $I \sim q^{-1}$ whereas the latter shows $I \sim q^{-2}$ characteristic of a layered structure (vesicles were observed by cryo-TEM) [116]. These lipopeptides are of interest due to their interaction with the model pesticide glyphosate [*N*-(phosphonomethyl) glycine] and as a potential colorimetric detection system. Thus, SAXS was also used to probe the effect of the pesticide on the peptide aggregates, a transition to spherical micelles being observed for PRWG-C_{18} but no transition was noted for PRWG-$(C_{18})_2$ [116]. The ordering of residues in lipopeptide homologues (constitutional isomers) also influences their self-assembly as probed by SAXS form factor features, as exemplified by SAXS data for C_{16}-VEVEGRGD compared to C_{16}-VVEEGRGD [117].

A range of downloadable software is now available to analyse and fit SAS data. Lists are available in the literature [39,55]. We have extensively used the software SASfit [118] to fit form factor data from amphiphilic peptide assemblies. The software includes many different form factors including those described above and many others, and it also has a powerful least-squares fitting algorithm. Other software to fit SAS data is available including SASView [119], GENFIT[120] or FISH (SANS specific) [121]. In addition, software is available to calculate SAS profiles from pdb files (which can be constructed or generated from simulations of peptide assemblies) including CRYSOL [122]/CRYSON (x-ray and neutron versions) available within the ATSAS SAS data analysis and modelling package [123] and FoXS [124,125], and others [126]. More information on these methods is provided in Section 2.3.

2.2. Structure factors

Structure factor effects for peptides in solution are observed at higher concentration (and also in gels) and lead to peaks in small-angle scattering data. In more highly ordered soft materials, series of Bragg peaks are observed that provide information on the nanostructure [39,127].

The pH-dependent self-assembly into spherical micelles, cylindrical micelles and hexagonal-packed cylinders (showing structure factor peaks) has been examined using SAXS for double tailed (C_{12} chains) lipopeptides bearing 18-residue intrinsically disordered peptide sequences [128,129]. Singular value decomposition (SVD) was used to determine the number of components present at pH values corresponding to morphological transition regimes. Interestingly, longer chained lipopeptide analogues (with C_{14} chains) can form FCC or BCC cubic phases (at 5 mg/ml concentration) with speckle-like ('powder diffraction') SAXS patterns with multiple rings of reflections [129]. Lipopeptides comprising four heptyl chains can form lamellar phases depending on conditions of pH or salinity [128].

SANS was used to probe the order within hydrogels (in D_2O with buffer) of the VKVKVKVKV^{D}PPTKVEVKVKV-NH_2 containing a central β-hairpin V^{D}PPT motif. The data were fitted to a structure factor comprising a low q power law scaling of the intensity (Porod-type scattering) combined with a Lorentzian to describe the scattering at high q [130]. A similar model has been used with a low q power law and a Lorenzian function to account for the 'polyelectrolyte hole' peak observed by SAXS for charged homopolypeptides poly(L-arginine) and poly(L-glutamic acid), and their mixtures although an additional form factor term is required at high q to account for wormlike chain local structure (excluded volume) [131] effects [132]. A related model was used to fit SAXS data for poly(L-lysine)/poly(D-glutamic acid) with a low q power law and a wormlike chain form factor and a PRISM (Polymer Reference Interaction Site Model) structure factor [133].

The presence of a structure factor peak is a feature of peptide gels and the peak position is related to the mesh size in the gel (e.g. spacing between peptide fibrils), while the peak width is related to the correlation length. Such peaks are often fitted using generic peak functions such as a Gaussian or Lorentzian. In one example, a function containing modified Lorentzian (with variable power of q in the denominator) has been used to fit SANS data from the bola-amphiphile $DGRL_4DGW$ in D_2O, enabling determination of the mesh size (correlation length) [134]. Kratky plots also revealed that the degree of folding of peptide fibrils in the hydrogels decreases at higher temperatures. In another example, contrast variation SANS showed a peak due to inter-fibril correlations in hydrogels formed by a PNIPAM-FEFEFKFK conjugate with a deuterated poly(*N*-isopropylacrylamide) (PNIPAM) chain linked to the model β-sheet peptide FEFEFKFK [113]. The scattering arising from the non-deuterated peptide component with much higher contrast than that of the deuterated polymer with respect to the D_2O solvent led to the peak which enabled the mesh size to be determined.

SAXS has been used to probe the fibrillar nanostructure within peptide conjugate hydrogels such as those formed by naphthalene diimide-histidine bola-amphiphiles [135]. or telechelic YY-PEG-YY conjugate (with PEG M_w = 1500 $gmol^{-1}$) [136]. In another example, SAXS revealed the lamellar structure in hydrogels of lipopeptide derivatives of phenylalanine or tryptophan, from which the molecular packing could be modelled [137]. Similar SAXS data showing Bragg peaks was obtained for histidine-derivative peptide and lipopeptide hydrogels [138,139].

A number of lipopeptides have been shown to form multi-lamellar nanosheet or nanotape structures in aqueous solution. One example is C_{16}-KTTKS which is a commercial lipopeptide from the Matrixyl™ family of collagen-stimulating lipopeptides used for anti-wrinkle skincare applications. This molecule shows strong Bragg peaks in SAXS patterns, which exhibit alignment under flow of the peptide nanotapes which comprise a stack of interdigitated bilayers (Fig. 5) [140]. SAXS also shows that the lamellar phase melts on heating and spherical micelles are formed (spherical micelles are also formed at room temperature upon reduction of pH [141]). The lipopeptides C_{16}-KT (containing a shorter fragment of the procollagen-derived KTTKS sequence) and C_{16}-GHK also show Bragg peaks in SAXS patterns, due to proposed lamellar bilayer structures [142] The lipopeptide C_{16}-βAH containing the bioactive carnosine (β-alanine-histidine) dipeptide also shows SAXS patterns with Bragg peaks corresponding to layered structure within the observed nanotapes [77]. Its interaction with multilamellar vesicles of the lipid dipalmitoylphosphatidylcholine (DPPC) were also studied by SAXS. The peptides RF and $[RF]_4$ induce a transition from multilamellar to unilamellar vesicles of DPPC as shown by SAXS [143].

The interaction of peptides with lipid membranes (vesicles) has been probed via SAXS and SANS, especially for cationic peptides and peptide conjugates interacting with anionic or zwitterionic membrane models of bacterial or mammalian cell membranes. Such peptides have been

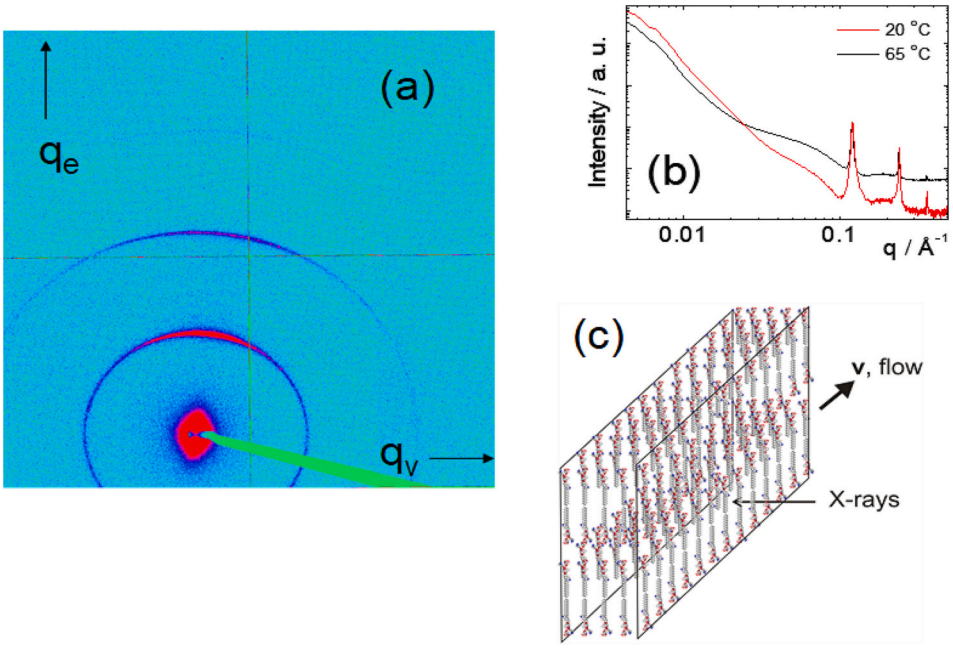

Fig. 5. SAXS data and model of bilayer structure for C_{16}-KTTKS in aqueous solution. (a) 2D SAXS pattern showing spontaneous alignment of flow-aligning nanotapes, q_e and q_v indicate the wavevectors along with neutral and flow velocity directions, (b) 1D SAXS profiles at 20 °C showing lamellar structure and 65 °C with a micellar form factor, (c) Schematic of bilayer packing in nanotape (also showing alignment direction). From reference [140].

studied due to potential antimicrobial or cell-penetrating activity. Multilamellar vesicles will produce a SAS profile containing Bragg peaks, whereas unilamellar vesicles have a SAS form factor arising from the layer structure, which can be described with a Gaussian bilayer model used for nanotape structures, as discussed in the previous section. Our group has extensively used SAXS to probe the interaction with a number of arginine-functionalized surfactant-like peptides (SLPs) e.g. A_6R [144,59]. A_9R [145], RA_3R [146], RA_6R [147], RA_9R [147], R_3F_3 [82] or R_4F_4 [82], among others) with model lipid membranes including several anionic phosphoglycerol (PG), or zwitterionic phosphoethanolamine (PE) or phosphocholine (PC) lipids (as mimics of anionic bacterial or zwitterionic eukaryotic membranes). Arginine can form bidendate hydrogen bonds with the phosphate groups within lipid headgroups [148]. The arginine-rich SLP peptides are of interest due to antimicrobial activity against a range of pathogens. Fig. 6 shows representative SAXS data for lipid vesicles in the presence of A_6R (capped at both termini). The SAXS data for capped A_6R itself (above the critical aggregation concentration) was fitted using a cylindrical shell form factor [59]. whereas the uncapped peptide shows SAXS form factor features of nanotapes or nanotubes (at higher concentration) [78]. The data in Fig. 6 are for two types of mixture POPG/ POPE and DOPC/POPC (full lipid names given in figure caption), the former are anionic mimics of bacterial membranes and the latter are zwitterionic lipids as a mimic of eukaryotic membranes. The POPG/POPE mixed vesicles are initially unilamellar as shown by the SAXS data in Fig. 6a, however addition of the peptide leads to a restructuring to multilamellar vesicles as shown by the development of Bragg peaks. In contrast, the DOPC/POPC vesicles are multilamellar, but there is a decorrelation of lipid bilayers and loss of structure factor peaks upon addition of the peptide [59].

Time-resolved SANS H/D exchange experiments have been used to investigate the influence of antimicrobial peptides on lipid membranes and the associated kinetic processes [149,150]. Fig. 7 shows time-resolved SANS profiles for H/D exchange due to lipid flip/flop in mixtures with and without the antimicrobial peptide indolicidin [150]. The experiment involves studying the change in contrast upon mixing deuterated and nondeuterated vesicles as shown in Fig. 7a. Lipid exchange leads to reduced contrast, tending towards matching with the 50% H_2O/50% D_2O solvent. The lipids studied were mixtures of DMPC

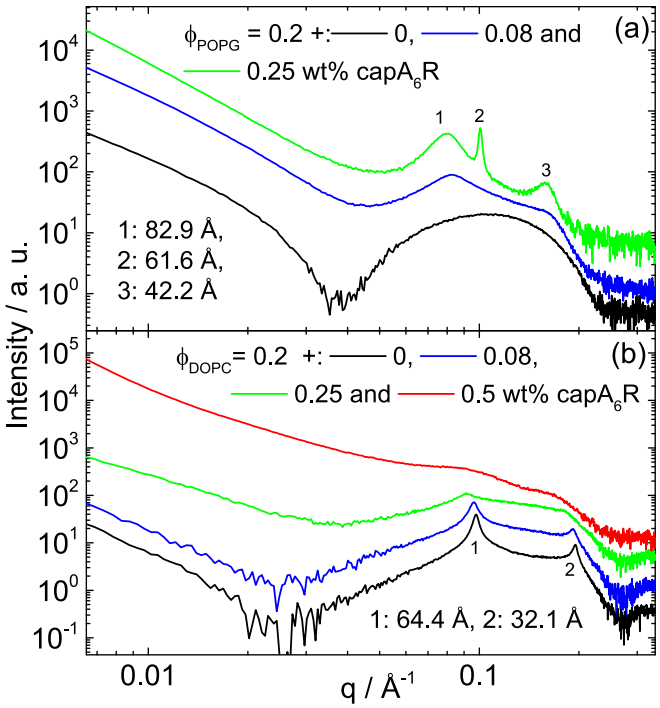

Fig. 6. SAXS data measured for vesicles with (a) ϕ_{POPG} = 0.2 and (b) ϕ_{DOPC} = 0.2, mixed with 0.08, 0.25 or 0.5 wt% A_6R (capped peptide Ac-A_6R-NH_2). Here ϕ_{POPG} denote the fractional content of POPG (2-oleoyl-1-palmitoyl-*sn*-glycero-3-phospho-rac-(1- glycerol) sodium salt in mixtures) in mixtures with POPE (2-oleoyl-1-palmitoyl-*sn*- glycero-3-phosphoethanolamine. Correspondingly, ϕ_{DOPC} is the fractional content of DOPC (1,2-dioleoyl-*sn*-glycero-3-phosphocholine) in mixtures with POPC (2-oleoyl-1-palmitoyl-*sn*-glycero-3-phosphocholine). The SAXS data has been multiplied by an arbitrary factor to aid visualization of the data. Bragg peak spacings are indicated. From reference [59].

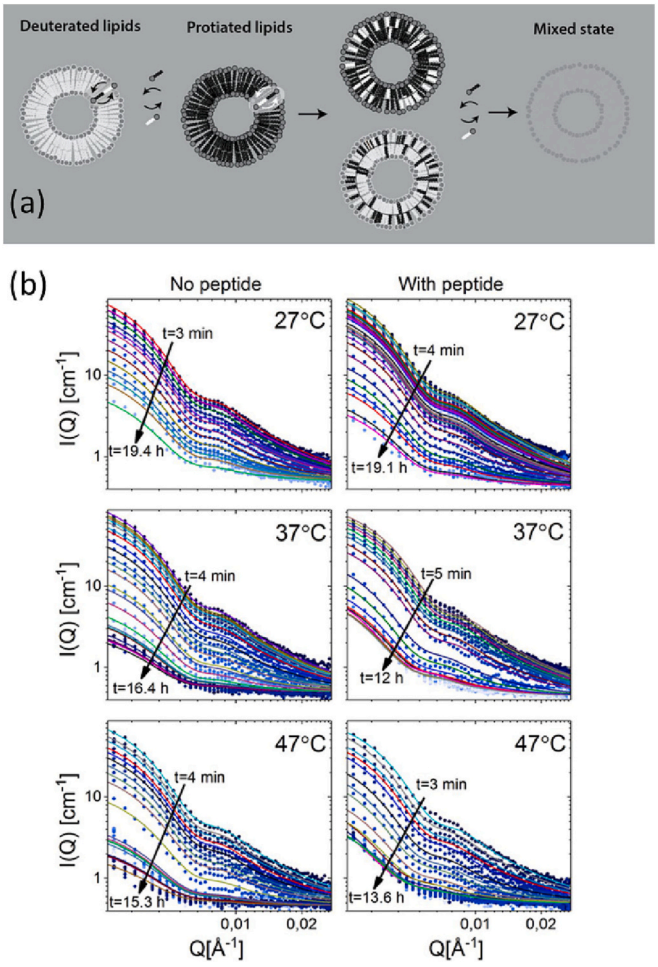

Fig. 7. Time-resolved SANS data due to H/D exchange in mixed lipid vesicles. (a) Scheme of process. (b) SANS profiles for mixed DMPC/DMPG vesicles (with small amounts of DMPE-PEG stabilizer) over the timescales (and at the temperatures) indicated with changes resulting from reductions in contrast and increase in radius of vesicles with and without added antimicrobial peptide indolicidin (1:20 ratio). From reference [150].

(1,2-dimyristoyl-*sn*-glycero-3-phosphocholine) and DMPG (1,2-dimyristoyl-*sn*-glycero-3-phospho-(1′-rac-glycerol)) (in a 75 mol% to 22.5 mol % ratio), with DMPE-PEG (1,2-dimyristoyl-*sn*-glycero-3-phosphoethanolamine-*N*-[methoxy(polyethylene glycol)-2000]) (2.5 mol%) as PEGylated vesicle suspension stabilizer. The starting vesicles are mixtures of DMPC and DMPG (protonated vesicles) and perdeuterated d_{54}-DMPC and d_{54}-DMPG as deuterated vesicles (both with DMPE-PEG stabilizer). The data in Fig. 7b shows that the radius of the vesicles increases with time, and fitting analysis of the overall H/D contrast reduction enables the flip-flop rates to be obtained. The antimicrobial peptide accelerates lipid transport and additionally limits vesicular growth [150]. The presence of laterally phase separated domains ('rafts') in the mixed lipids was excluded on the basis of SANS under contrast matching conditions [151]. In an earlier study, SANS was used to investigate the effect of peptide hormone angiotensin II on the structure of unilamellar d_{54}-DMPC vesicles [152].

The arginine-rich cell-penetrating peptide KKRRQRRR sequence from the HIV TAT protein domain can induce negative Gaussian curvature in membranes from mixed anionic phosphoserine and zwitterionic phosphoethanolamine lipids, leading to the formation of cubic phases ($Pn\bar{3}m$) as shown by SAXS profiles containing many orders of reflection (Fig. 8) [153,154]. Machine learning on antimicrobial peptides (with 8-60 residues, from the antimicrobial peptide database)

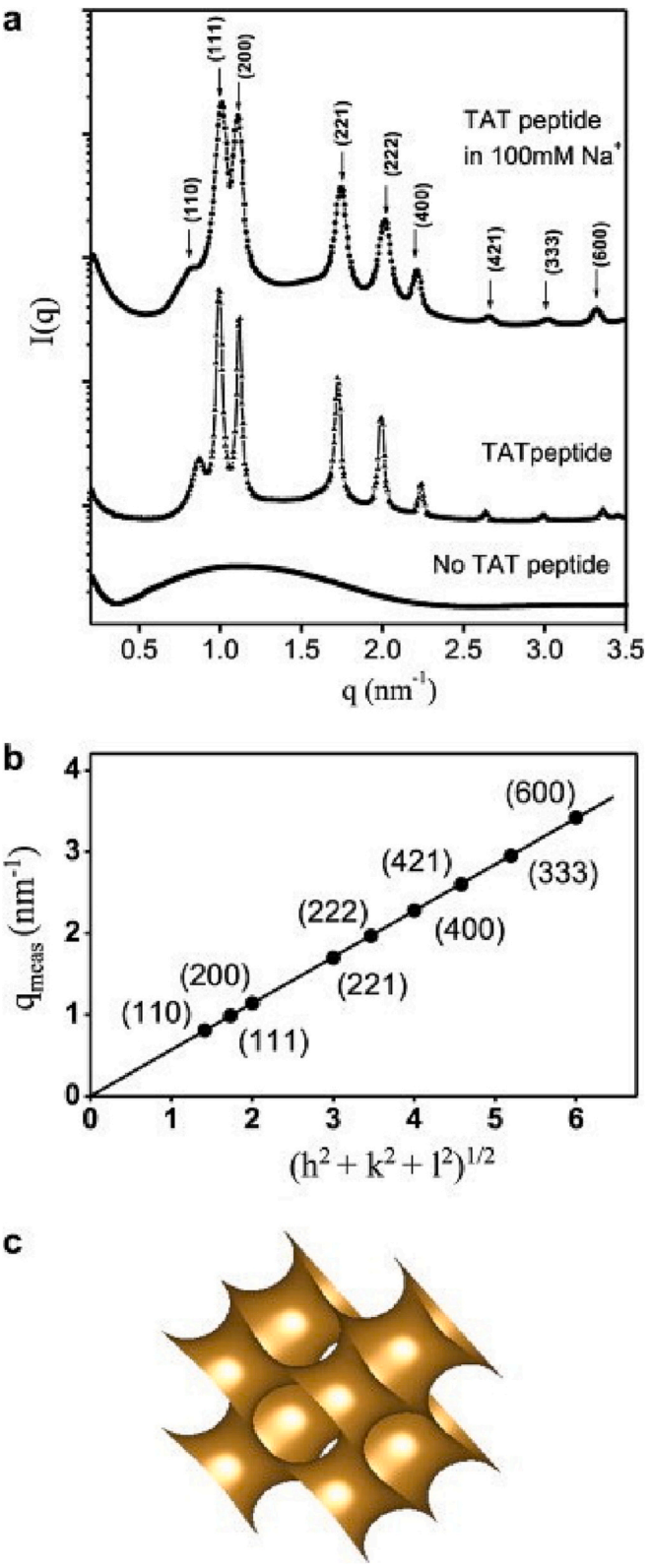

Fig. 8. SAXS from the TAT cell-penetrating peptide with a mixed zwitterionic/anionic lipid system, (a) SAXS data showing Bragg peaks induced by the peptide causing curvature of the lipid membrane and bicontinuous cubic phase formation, (b) Indexation of the peaks indicates a 'double diamond' $Pn\bar{3}m$ structure with lattice parameter $a = 10.97$ nm, (c) Schematic of the corresponding bicontinuous cubic phase. From reference [154].

enabled identification of a parameter which by comparison with experimental SAXS data and antimicrobial activity (growth inhibition assays) was found to relate to the propensity to form negative Gaussian curvature in bacterial membranes [155].

The Stupp group have used SAXS in their studies on the formation of hybrid membranes formed by complexation of self-assembling lipopeptides with oppositely charged polysaccharides such as hyaluronic acid (HA), heparin or alginate. Membranes with an inner structure of fibrils perpendicular to the surface are formed by mixing a heparin-binding lipopeptide C_{16}-A_4G_3LRKKLGKA with hyaluronic acid and heparin [156]. Actually, SAXS also revealed the time-resolved development of cubic ordering at a particular defined lipopeptide/HA concentration in heparin-free mixtures [156]. Complexation with HA was also studied for a photocleavable lipopeptide bearing a nitrobenzyl ester unit in the peptide backbone (which is responsive to UV light) and again SAXS was used to study the self-assembly of the PA before and after cleavage, as well as in sacs formed in the complexes with HA [157].

Complexation of cationic lipopeptides C_{16}-$V_3A_3K_n$ (with n = 2 for sample termed PAK2, n = 3 for PAK3 and n = 4 for PAK5) with elastin-like peptides (ELPs) leads to robust membranes, which can be manipulated to draw out tubes [158]. SAXS reveals that there is a lamellar structure within the tubes, as shown by the presence of Bragg peaks in the data (Fig. 9a). Meanwhile, SAXS reveals differences in conformation above the critical transition temperature (T_t) of the ELP for the ELP/lipopeptide mixtures compared to the ELP itself. Kratky plots [39] (q^2I (q) vs. q) of SAXS data show hydrophobic collapse is observed for the ELP, whereas an expanded conformation is present in the membranes containing lipopeptides (Fig. 9b) [158].

SAXS has been used to probe the order within planar or spherical membranes formed by β-sheet $PK(FK)_5P$ with alginate (an anionic polysaccharide). The preparation conditions and method (especially order of mixing) have a large influence on the presence of lamellar structure factor peaks in the SAXS data [159]. The peptide itself forms a nematic phase of fibrils (at 5 wt%) which spontaneously align, producing highly anisotropic SAXS patterns [160]. The development of anisotropy was observed during aging, over a period of several days. Analysis of Kratky plots for alginate/peptide gels show differences (presence or absence of a peak) depending on the peptide sequence when comparing peptides X_6KRGDY with X = G, A or V [161]. This indicates differences in the gel mesh structure, i.e. compactness or branch density of the gel crosslink regions. SAXS was used to determine the fibrillar structure in solutions of cationic peptides $K_2X_nF_4$ (X_n = A_3, A_5, A_7, S_5 or G_7) used in the fabrication of membranes with HA, which SAXS showed are characterized by Bragg peaks characteristic of the average mesh size [162].

At most synchrotron SAXS beamlines (and on many lab instruments) and SANS instruments the data is measured on a 2-dimensional area detector and it is straightforward to check for sample alignment which is manifested in anisotropy in the SAS pattern. In some cases, spontaneous alignment of the sample is observed. This has been noted for several peptide and lipopeptide samples (forming aligning fibril or nanotube structures) when flowing them through a capillary at SAXS and BioSAXS beamlines (as mentioned for example in the discussion of Fig. 5). However, orientation is best studied under precisely defined flow conditions such as steady shear (with a Couette cell for example) or with simultaneous rheology and SAXS or SANS (rheoSAXS or rheoSANS). Representative SANS data obtained for a solution of RFL_4FR peptide nanotubes in a commercial rheometer are shown in Fig. 10 [91]. The SANS pattern (here the data correspond to the radial configuration where the beam passes through the centre of the Couette cell) develops anisotropy under steady shear, although this is lost upon cessation of

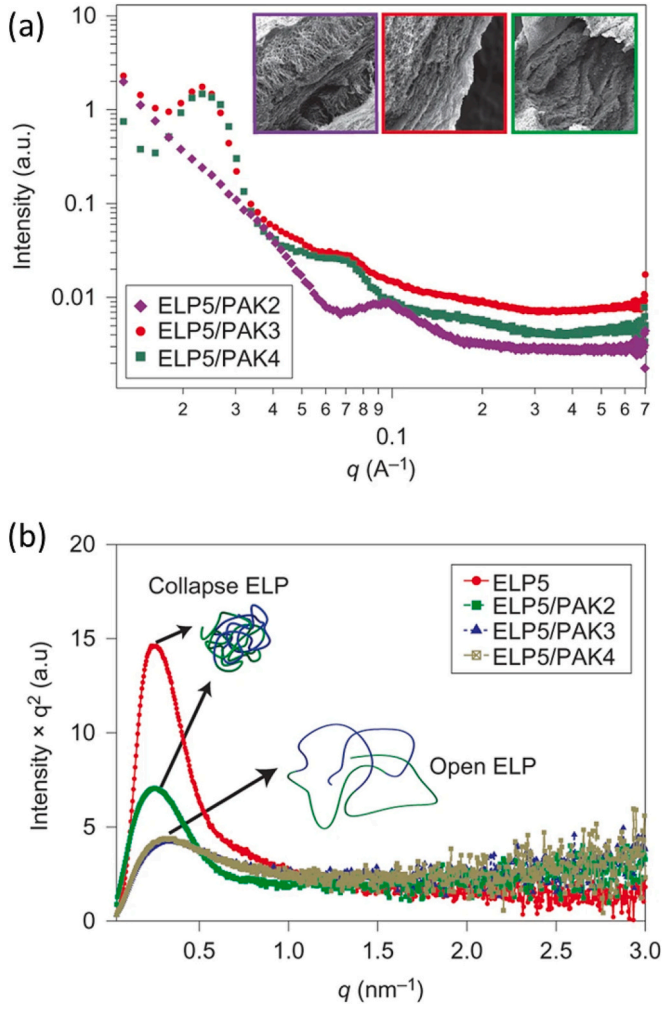

Fig. 9. SAXS data from mixtures of an elastin-like peptide (ELP5) with lipopeptides C_{16}-$V_3A_3K_n$ n=2 (PAK2), n=3 (PAK3) or n=4 (PAK4). (a) Bragg peaks from lamellar order within membranes (inset SEM micrographs, colour coded to correspond to SAXS curves), (b) Kratky plot of SAXS profiles above critical transition temperature, comparing ELP5 with mixtures of ELP5 with the lipopeptides. From reference [158].

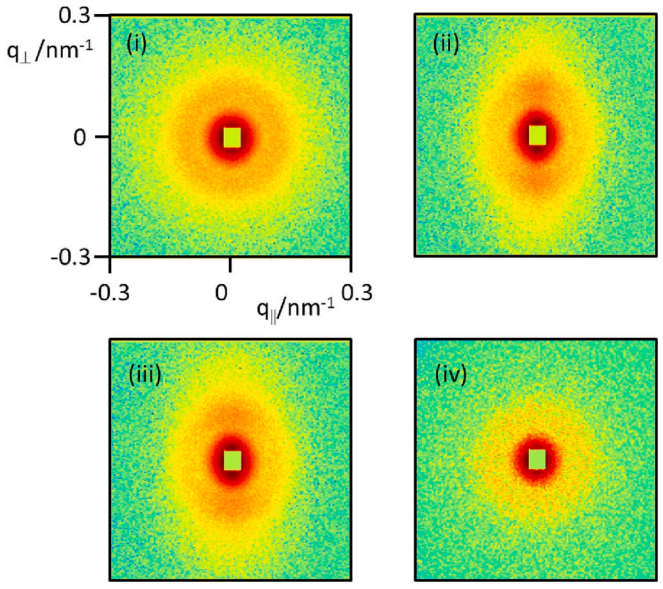

Fig. 10. SANS patterns obtained from a 1 wt% solution of RFL_4FR in D_2O in the radial configuration [91]. (i) Zero shear (ii) under shear at $\dot{\gamma}$ = 100 s^{-1}, (iii) under shear at $\dot{\gamma}$ = 1000 s^{-1}, (iv) Following shear at $\dot{\gamma}$ = 1000 s^{-1}. The shear direction is horizontal and the intensity scale is logarithmic.

shear (i.e. this sample only aligns under flow).

Certain peptides and peptide conjugates can form lyotropic liquid crystal phases (e.g. nematic, hexagonal-packed cylinder or lamellar) in high concentration solution (typically aqueous solution). These phases also have the tendency to align under flow. Examples of SAS data from such systems include anisotropic SANS and SAXS patterns measured for the amyloid peptide conjugate FFKLVFF-PEG (containing the KLVFF Aβ16-20 peptide and PEG3000) which forms flow-aligning nematic and hexagonal phases [72,73]. or the SAXS data showing hexagonal phase formation of cyclic peptide Lanreotide mentioned above [94]. Strongly anisotropic SAXS data is observed for aligned bundles of lipopeptide fibrils, prepared as 'strings' or 'noodles' by injection of the lipopeptide solution into buffer solution [163].

2.3. *Ab initio modelling of SAXS from peptide solutions*

As mentioned in Section 2.1, much software is available to analyse and model SAS data including methods to calculate SAS profiles from *ab initio* models. The most widely used is ATSAS, which is a comprehensive software package for SAS (mainly SAXS) data from biomolecules (especially proteins) in solution [123,164]. It comprises a series of routines to analyse and model SAXS data including *ab initio* methods. Several of these approaches are described below, as well as the literature [37,39,123,165]. In the following, some of the ATSAS routines have been superseded by those with other names as the package has developed.

For systems for which SAXS data for a multi-component system is additive, singular value decomposition (SVD) may be performed (a routine to do this is available in PRIMUS within the ATSAS package [164]). Examples of such systems include peptides where monomers aggregate into amyloid fibrils (intermediate oligomers can also be detected). This method has been used by Vestergaard and Otzen and their coworkers to investigate the aggregation of amyloid formed by a number of peptides including insulin [166], glucagon [167], α-synuclein [168]. and the yeast prion peptide GNNQQNY [169] Fig. 11 shows SAXS data obtained during the fibrillisation of insulin under acidic conditions. SVD indicated the presence of three species – monomers, oligomers and fibrils [166]. Ab initio shapes of the insulin fibril repeat unit and the oligomer were obtained using DAMMIN from ATSAS in which the scattering object is represented by a bead model which is iterated minimizing the discrepancy between the experimental and calculated SAXS curves. The search volume was first estimated using the program

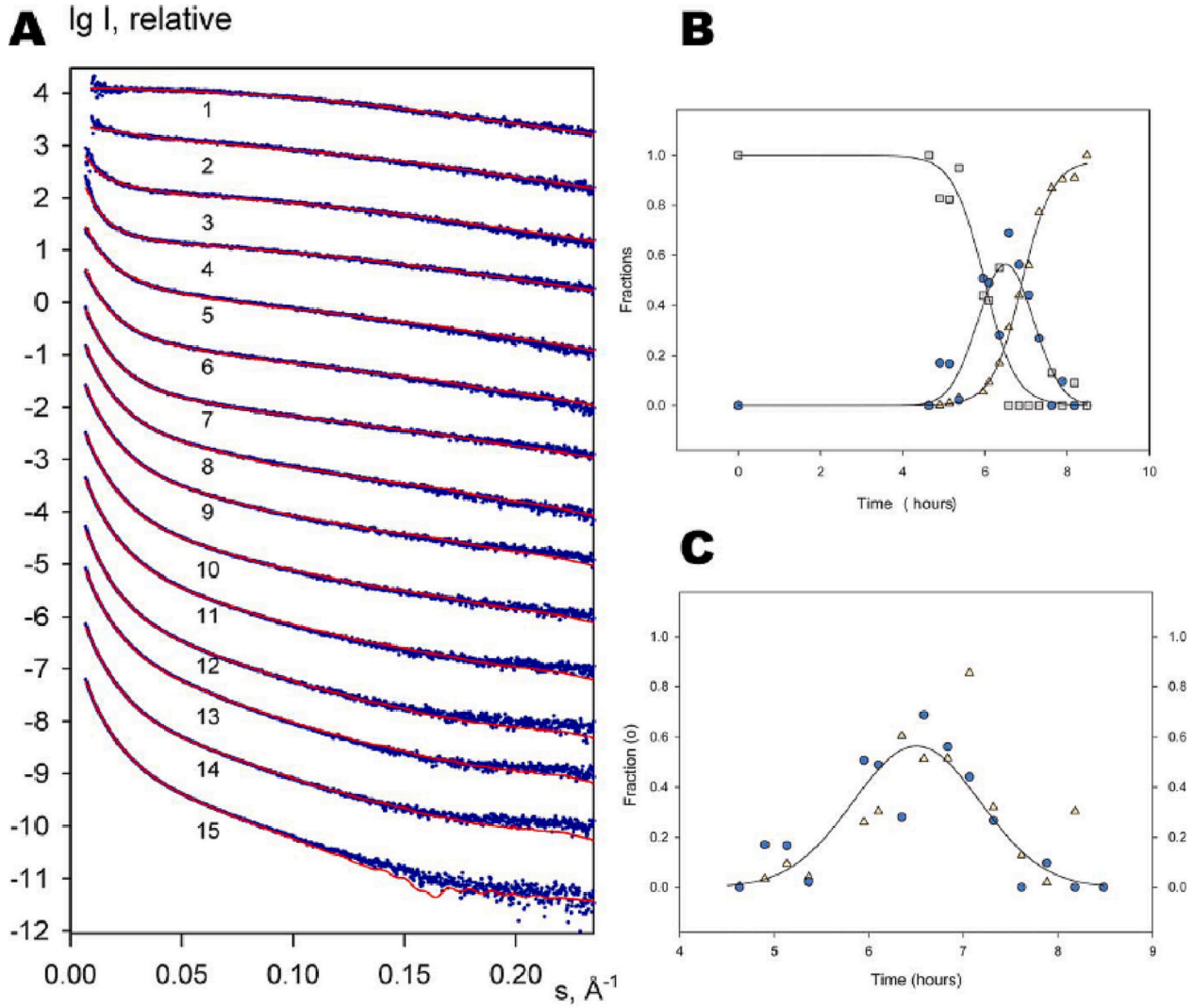

Fig. 11. A) SAXS data for insulin aqueous solution (pH 2, with NaCl, T = 45 °C) as a function of time (in h, the successive curves labelled 1 to 15 are displaced by one logarithmic unit for clarity). Blue dots: experimental data, red lines: fits for the three-component mixtures (for the bottom curve, a fit from an *ab initio* shape model obtained for fibrils is displayed, B) Relative fractions of components present. Grey squares: insulin monomer, blue circles: helical oligomer, beige triangles: fibril. C) Comparison of oligomer fraction (blue circles and fitted curve) with rate of formation (first derivative) of fibril component (beige triangles). Reproduced from ref [166].

BODIES, and averaged bead models (20 independent models) were calculated using DAMAVER. The oligomer structure was modelled as a helical structure [166]. DAMMIN and DAMAVER were also used to generate *ab initio* SAXS intensity curves for glucagon [167]. For the oligomer, such models (produced using DIMFOM) were compared to those generated from the pdb file of the crystal structure (using CRYSOL). For the fibril, bead models based on stacked hexamers with a fibril twist were also used to calculate SAXS curves [167]. Small aggregates up to hexamers were detected in the early oligomerization stage (lag phase before fibrillization), for which concentration-dependent data were analysed using a generalized indirect Fourier transform (GIFT) method [170], which provides the pair distance distribution function. In another case, *ab initio* calculations based on atomic coordinates from MD simulations were used to compute (via the Debye formula) the SAXS profile for micelles of C_{16}-IKPEAP using the software FoXS [124,125], usually used for proteins but which can compute solution SAXS from a pdb of a globular structure such as a micelle as well, provided the shell hydration layer is adequately represented [171].

3. SAXS/WAXS

Combined (simultaneous) SAXS/WAXS is available on several synchrotron beamlines internationally, as well as some lab instruments. It has been used in a relatively small number of studies on peptide materials to probe the order on multiple lengthscales, in particular the nanostructure from SAXS and the local molecular packing (e.g. secondary structure) from WAXS or hierarchical order in conjugates where the non-peptide component may show local ordering, for instance in a crystalline polymer. A few selected examples are described in the following.

SAXS and WAXS have been used to probe the hierarchical order within hybrid membranes formed in mixtures of the cationic lipopeptide C_{16}-KKFF with alginate [172]. Soft membrane sacs are formed by electrostatic complexation with this polyelectrolyte (cf. discussion in Section 2.2) but addition of graphene oxide (GO) leads to capsule formation. The capsules can be further stiffened by addition of $CaCl_2$ producing self-supporting capsules. Fig. 12 shows images of the sacs and capsules along with SAXS and WAXS data. The Bragg peak in the SAXS profile for each sample arises from a layered structure and the WAXS data shows reflections from GO and/or sodium alginate along with a 4.4 Å peak due to the β-strand spacing within a β-sheet structure (except for the stiffer capsules) [172]. Neutron fibre diffraction (wide-angle neutron scattering) can similarly provide information on peptide secondary structure, such as that of amyloid fibrils [173].

The combination of SAXS and WAXS provides *in situ* information on the hierarchical order within hydrogels of fibril-forming surfactant-like

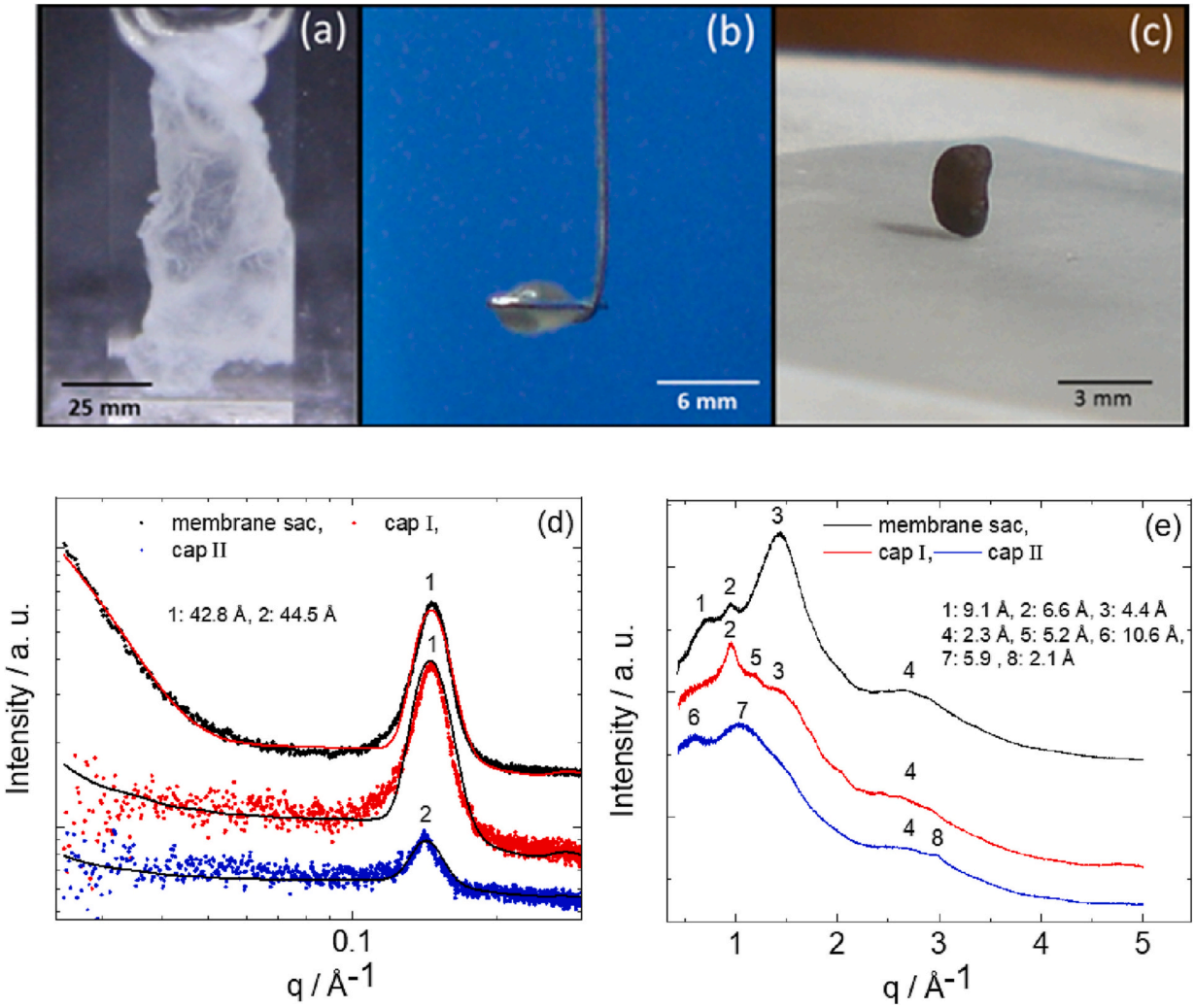

Fig. 12. Images and SAXS/WAXS data from hybrid capsules formed by hybrids lipopeptide C_{16}-KKFF with sodium alginate, producing soft sacs and with additional graphene oxide (GO) producing capsules of type cap I) and GO + $CaCl_2$ producing self-supporting stiff capsules (cap II). (a–c) Images: (a) membrane sac, (b) cap I, (c) cap II, (d) SAXS profiles – open symbols: measured data, lines: lamellar structure factor/bilayer form factor fits, Bragg peak spacings indicated, (e) WAXS data with indexed reflections. Reproduced from ref [172].

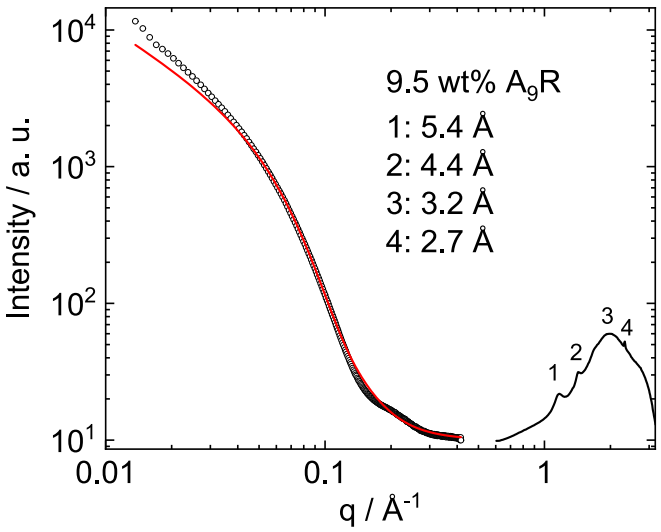

Fig. 13. Combined SAXS/WAXS data from a hydrogel of surfactant- like peptide A_9R (9.5 wt% in water). The SAXS data (open symbols) is fitted with a core-shell cylinder form factor (red line), the WAXS data provides *in situ* data showing peaks indicating a β-sheet structure within the fibrils [145].

peptide A_9R (Fig. 13) [145]. The SAXS data can be fitted to the form factor of a cylindrical shell, while the WAXS data contains peaks from the β-sheet structure (5.4 Å oligo-alanine β-sheet spacing and 4.4 Å β-strand spacing with other intra-sheet spacing peaks). Combined SAXS/WAXS has also provided detailed information on the packing of A_6K in nanotubes, since WAXS on partly oriented samples gives information on molecular packing in the tube wall [93,174]. WAXS (actually extended q range SAXS) reveals a peak due to α-helical ordering in a different class of peptide nanotubes formed by the self-assembly of surfactant-like peptide R_3L_{12} into nanotubes [175]. In situ SAXS/WAXS on lipopeptide C_{16}-ETTES designed in our group as an analogue of the Matrixyl^{TM} lipopeptide C_{16}-KTTKS shows a SAXS profile with Bragg peaks from a lamellar structure (actually coexisting hydrated and dehydrated lamellar structures were proposed), while the WAXS peaks are consistent with β-sheet ordering of the peptide [176]. Co-assembly in mixtures of C_{16}-ETTES and C_{16}-KTTKS leads to SAXS profiles showing Bragg peaks. Another study used SAXS/WAXS to probe ordering of β-sheet fibrils containing light neurofilament chain peptide coupled with biotin or the fluorescence label 5-carboxy-fluorescein [177]. SAXS shows a peak due to lateral packing and the WAXS data contain a peak due to β-sheet ordering (which was observed to be aligned in a 2D pattern obtained from a dried sample). Such a peak has also been observed for peptide F_4R_4 at sufficiently high concentration in aqueous solution [103]. Synchrotron SAXS/WAXS provided unique insights into the transition to nanoscrolls observed for the cationic cyclic peptide Lanreotide (Section 2.1) in mixtures with anionic lipids, a thermal lipid gel-to-fluid lipid phase transition within the nanoscrolls being observed by WAXS, with concomitant changes in the SAXS peaks [178].

Synchrotron SAXS/WAXS has provided valuable *in situ* insight into the ordering of several other bioactive lipopeptides. Mixtures of β-sheet-forming lipopeptide $E_3A_3V_3$-C_{16} with the constituent $E_3A_3V_3$, E_3A_3 or E_3 peptides (none of the peptides themselves form β-sheet structures, as shown by WAXS) were investigated using techniques including SAXS/WAXS as part of a study of co-assembly [179]. This revealed that the lipopeptide fibrils can incorporate the peptides at low content but at higher concentrations copolymerization of peptide and lipopeptide is observed with disrupted β-sheet secondary structure [179]. This is illustrated in a schematic in Fig. 14 which also shows SAXS data for annealed and unannealed samples, with better defined form factor minimum in the former case (and a slightly different low *q* scaling) together with VT-WAXS (VT: variable temperature) which shows the development of β-sheet peaks upon annealing (heat-cool treatment) [179]. In a further example, SAXS/WAXS and cryo-TEM reveal differences in the final morphology (fibrils/twisted ribbons) of model β-sheet lipopeptides C_{16}-AAEE and C_{16}-AEAE depending on the preparation method (addition of salt and or high temperature annealing and the ordering of these treatments) [180]. VT-WAXS showed the disappearance of the β-sheet features on heating and their pathway-dependent reappearance or otherwise on cooling. SAXS/WAXS has also been used to probe the hierarchical order in mixtures of oppositely charged lipopeptides which form different fibril morphologies depending on pH as electrostatic interactions are modulated [181]. The 'cohesiveness' of aggregates was also tuned via incorporation of β-sheet domains between the lipid chain and charged terminal domain. This influences both the SAXS profile due to the formation of cylindrical or flat (nanotape) structures (and also the extent of bundling of these aggregates) and the intensity and/or position of WAXS peaks (which in some cases show lattice ordering of β-strands) [181]. A hexagonal phase was observed for lipopeptide C_{16}-A_3E_3 by SAXS, and WAXS showed a peak due to the 4.6 Å β-sheet repeat [182]. This lipopeptide spontaneously forms a hexagonal phase at high concentration but also x-ray induced hexagonal ordering was observed at lower concentration (1 wt% aqueous solution) due to beam damage which leads to ionisation, which in turn was proposed to lead to ordering of peptide nanostructures due to increased charge density on the fibrils [182].

SAXS/WAXS sheds light onto an interesting interplay between amyloid fibrillization tendency and PEG crystallization in conjugates containing the KLVFF peptide from Amyloid β (Aβ16–20) conjugated to PEG with molar mass 3300 g mol^{-1}. The peptide KLVFF is a weak fibrillizer whereas the N-terminal modified variants FFKLVFF and AAKLVFF have a stronger aggregation tendency. PEG crystallization can overcome the fibril formation of KLVFF leading to a Bragg peak in the SAXS data due to the formation of a semicrystalline lamellar structure of PEG whereas there is no such peak for FFKVFF-PEG or AAKLVFF-PEG (Fig. 15a) [183,184]. The structure of strong fibrillizing peptides is not disrupted by PEG crystallization in the latter two samples. Temperature-ramp SAXS/WAXS shows the reversibility of the morphology change in SAXS as well as the PEG crystallization detected by WAXS (Fig. 15b). Low molar mass PEG has less tendency to crystallize, this is confirmed by studies on dried samples of PEG_n-F_6 (n = 8, 12, 18, 24, and F_6 denotes hexaphenylalanine) for which WAXS and GIWAXS on dried samples show β-sheet features, not peaks due to PEG crystallization [185].

4. Concluding remarks

The examples highlighted herein show that small-angle scattering techniques are well suited to provide information on the shape and dimensions of peptide nanostructures. SAXS is more widely available and so is more commonly used, however SANS has unique advantages since it is possible to change contrast in a straightforward fashion using mixtures of solvents (herein, H_2O and D_2O) or by deuterium labelling of the peptide or peptide conjugate. Wide-angle scattering gives additional data on ordering at the local scale, i.e. on secondary structure or local organization in conjugates such as those containing crystalline polymers.

The future holds great promise for new developments in SAS measurement techniques arising from improvements in the source, sample environment, detectors and data analysis and modelling. Faster kinetic measurements will become possible at synchrotrons [186–188] and neutron sources [189] as they are developed, and as XFEL (x-ray free-electron laser) SAS is further explored [190]. Recently, synchrotron SAXS has enabled the dynamics of biomolecules (especially of proteins and their complexes and in particular of conformational flexibility) [39,48,191–194] to be probed and it will be interesting to extend such measurements to investigate the dynamics of peptide self-assembly. This will shed light onto self-assembly processes, for example on- and off-pathway mechanisms of amyloid formation by β-sheet peptides

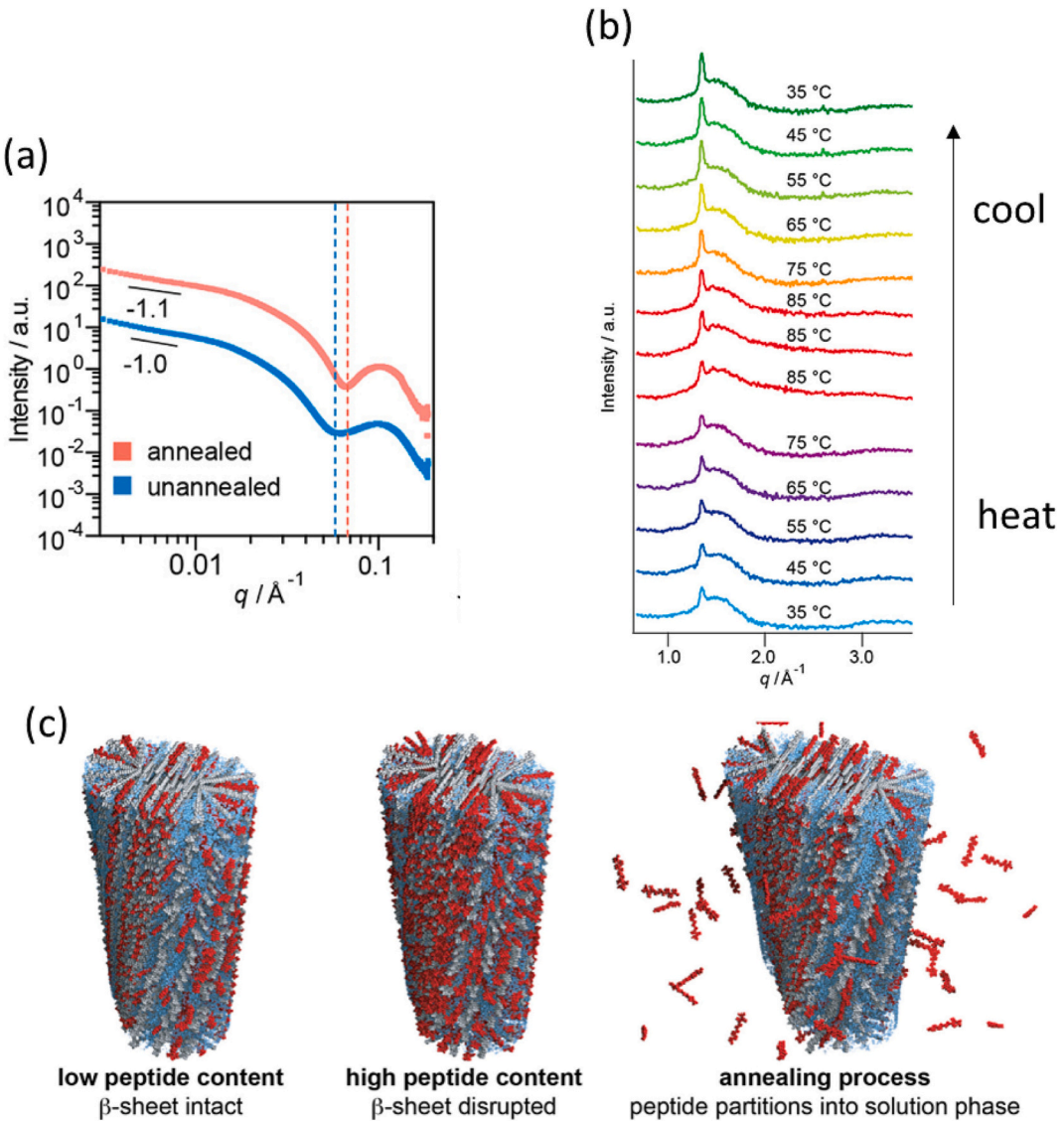

Fig. 14. SAXS/WAXS data from mixtures of lipopeptide $E_3A_3V_3$-C_{16} with peptide $E_3A_3V_3$ (1: 0.4 lipopeptide: peptide). (a) SAXS for annealed and unannealed samples showing differences in the width of the form factor minimum (dashed lines) and low q slope (shown), (b) VT-WAXS data during a heat-cool cycle showing development of β-sheet peak at $q = 1.35$ Å^{-1}, (c) Schematic of co-assemblies of peptide (red) and lipopeptide (grey). From reference [179].

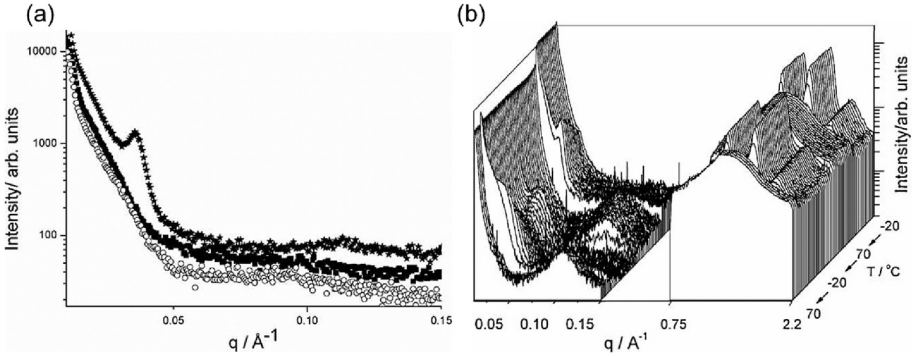

Fig. 15. Combined SAXS/WAXS data for PEG-peptide conjugates (with PEG 3300 g mol^{-1}) containing the KLVFF amyloid sequence from the Amyloid β peptide [183]. (a) SAXS profiles at 20 °C for (*) KLVFF-PEG, (■) AAKLVFF-PEG, (o) FFKLVFF-PEG, (b) Temperature-ramp SAXS/WAXS for KLVFF-PEG (heating at 2 °C with 5 min hold at intermediate temperatures -20 and 70 °C) showing successive melting and recrystallization.

(relevant to disease) [50,195] or the dynamics of lipopeptide self-assembly which have been shown to influence their properties [196,197]. It will also enable the elucidation of the fundamental processes of self-assembly (*n*-dimensional aggregation, nucleation and growth or coalescence or phase separation mechanisms etc) which for peptides will differ from other systems due to their unique patterns of hydrogen-bond interactions. Laboratory SAXS instruments are also showing significant improvements in performance with new x-ray source and detector technologies for example. This enables faster kinetic measurements as well as improved signal-to-noise, especially important for weakly scattering samples.

As discussed in Section 2.2, Time-resolved SANS (H/D exchange) has been employed to study the kinetics of self-assembly/morphology transition in amphiphilic molecules [39,198–201]. and this type of measurement is of great interest for peptide assemblies. As mentioned in Section 2.1, there is also a lack of studies exploiting the potential of deuteration to study the localization via contrast variation SANS of particular regions of peptide molecules within self-assembled structures.

Methods that are so far relatively underused in the peptide field will be taken up more widely. One example is anomalous small-angle x-ray scattering (ASAXS) (in which the scattering contrast is varied near the absorption edge of particular elements by changing x-ray wavelength [39]. which could be used to probe the distribution of particular ions around peptide structures, as used for nucleic acids [202,203] and other systems [204]. Another example is microfocus (also known as microbeam) scattering [39,46,205,206] (for instance to scan texture in peptide-based materials such as gels and films). GISAXS and GISANS may also be used more widely than the limited studies to date to examine peptide structures at surfaces (solid surfaces or air/water interfaces. For example, GISAXS has been used to probe peptide/lipid membrane interactions [207,208] and GISANS has been used to study shear alignment of peptide bola-amphiphile nanotubes [91].

Technical developments in other complementary methods such as electron microscopy will also enhance the analysis of better SAS data. The development of high resolution cryo-TEM methods, now widely used for protein structures, also has great potential to shed light on peptide nanostructures *in vitro*, providing a valuable complement to SAS data, for instance in terms of improved constraints in modelling SAS data. Better molecular modelling (e.g. molecular dynamics simulations of larger scale structures) will also aid in the analysis of SAS data. We can also look forward to new developments in data analysis and modelling, for example using machine learning techniques [155,209,210].

Novel peptides and conjugates will be developed with new functions and their activities (for instance in next-generation peptide therapeutics or in biomaterials for tissue engineering and other applications) may relate to nanostructure uncovered by SAS. New sample environments and the possibility for new types of *in situ* measurement under different conditions (for example fast mixing cells, novel sample cells to study peptide-based biocatalysts, to study hydration and many others) hold great potential [211]. In summary, there are many fruitful avenues for future research on peptide assemblies using small-angle scattering methods.

Declaration of Competing Interest

No.

Data availability

No data was used for the research described in the article.

Acknowledgements

This work was supported by EPSRC (UK) Fellowship grant (reference EP/V053396/1) to IWH. We thank all our colleagues in the small-angle scattering community, especially the too numerous to mention local contacts at many SAXS and SANS instrument beamtime sessions that our group has benefited from over the years.

References

[1] Löwik DWPM, van Hest JCM. Peptide based amphiphiles. Chem. Soc. Rev. 2004; 33:234–45.
[2] Gazit E. Self-assembled peptide nanostructures: the design of molecular building blocks and their technological utilization. Chem. Soc. Rev. 2007;36(8):1263–9.
[3] Hamley IW. Peptide fibrillisation. Angew. Chem. 2007;46:8128–47.
[4] Löwik DWPM, Leunissen EHP, van den Heuvel M, Hansen MB, van Hest JCM. Stimulus responsive peptide based materials. Chem. Soc. Rev. 2010;39(9): 3394–412.
[5] Zhao XB, Pan F, Xu H, Yaseen M, Shan HH, Hauser CAE, et al. Molecular self-assembly and applications of designer peptide amphiphiles. Chem. Soc. Rev. 2010;39(9):3480–98.
[6] Cui HG, Webber MJ, Stupp SI. Self-assembly of peptide amphiphiles: from molecules to nanostructures to biomaterials. Biopolymers 2010;94(1):1–18.
[7] Hamley IW. Self-assembly of amphiphilic peptides. Soft Matter 2011;7:4122–38.
[8] Trent A, Marullo R, Lin B, Black M, Tirrell M. Structural properties of soluble peptide amphiphile micelles. Soft Matter 2011;7(20):9572–82.
[9] Hamley IW. Peptide nanotubes. Angew. Chem., Int. Ed. Engl. 2014;53(27): 6866–81.
[10] Dehsorkhi A, Castelletto V, Hamley IW. Self-assembling amphiphilic peptides. J. Pept. Sci. 2014;20:453–67.
[11] Hamley IW. PEG-peptide conjugates. Biomacromolecules 2014;15:1543–59.
[12] Hamley IW. Lipopeptides: from self-assembly to bioactivity. Chemical Communications 2015;51:8574–83.
[13] Hutchinson JA, Burholt S, Hamley IW. Peptide hormones and lipopeptides: from self-assembly to therapeutic applications. J. Pept. Sci. 2017;23:82–94.
[14] Ke PC, Zhou RH, Serpell LC, Riek R, Knowles TPJ, Lashuel HA, et al. Half a century of amyloids: past, present and future. Chem. Soc. Rev. 2020;49(15): 5473–509.
[15] Zhang SG. Fabrication of novel biomaterials through molecular self-assembly. Nat. Biotechnol. 2003;21:1171–8.
[16] Löwik DWPM, Ayres L, Smeenk JM, van Hest JCM. Synthesis of bio-inspired hybrid polymers using peptide synthesis and protein engineering. Adv. Polym. Sci. 2006;202:19–52.
[17] Mart RJ, Osborne RD, Stevens MM, Ulijn RV. Peptide-based stimuli-responsive biomaterials. Soft Matter 2006;2:822–35.
[18] Cherny I, Gazit E. Amyloids: not only pathological agents but also ordered nanomaterials. Angew. Chem., Int. Ed. Engl. 2008;47:4062–9.
[19] Ulijn RV, Smith AM. Designing peptide based nanomaterials. Chem. Soc. Rev. 2008;37(4):664–75.
[20] Matson JB, Zha RH, Stupp SI. Peptide self-assembly for crafting functional biological materials. Curr. Opin. Solid State Mater. Sci. 2011;15:225–35.
[21] Jonker AM, Lowik DWPM, van Hest JCM. Peptide- and protein-based hydrogels. Chem. Mater. 2012;24(5):759–73.
[22] Matson JB, Stupp SI. Self-assembling peptide scaffolds for regenerative medicine. Chem. Commun. 2012;48(1):26–33.
[23] Fichman G, Gazit E. Self-assembly of short peptides to form hydrogels: design of building blocks, physical properties and technological applications. Acta Biomater. 2014;10(4):1671–82.
[24] Du XW, Zhou J, Shi JF, Xu B. Supramolecular hydrogelators and hydrogels: from soft matter to molecular biomaterials. Chem. Rev. 2015;115(24):13165–307.
[25] Tao K, Levin A, Adler-Abramovich L, Gazit E. Fmoc-modified amino acids and short peptides: simple bio-inspired building blocks for the fabrication of functional materials. Chem. Soc. Rev. 2016;45(14):3935–53.
[26] Wei G, Su ZQ, Reynolds NP, Arosio P, Hamley IW, Gazit E, et al. Self-assembling peptide and protein amyloids: from structure to tailored function in nanotechnology. Chem. Soc. Rev. 2017;46(15):4661–708.
[27] Sunna A, Care A, Bergquist PL. Peptides and peptide-based biomaterials and their biomedical applications. In: Advances in Experimental Medicine and Biology. Cham, Switzerland: Springer; 2017.
[28] Hamley IW. Small bioactive peptides for biomaterials design and therapeutics. Chem. Rev. 2017;17:14015–41.
[29] Hedegaard CL, Mata A. Integrating self-assembly and biofabrication for the development of structures with enhanced complexity and hierarchical control. Biofabrication 2020;12(3).
[30] Guler MO. Peptide-based biomaterials. In: Butt H-J, Hamley IW, Stone HA, Shen A, Edler K, editors. Soft Matter Series. Cambridge: Royal Society of Chemistry; 2021.
[31] Sheehan F, Sementa D, Jain A, Kumar M, Tayarani-Najjaran M, Kroiss D, et al. Peptide-based supramolecular systems chemistry. Chem. Rev. 2021;121(22): 13869–914.
[32] Ligorio C, Mata A. Synthetic extracellular matrices with function-encoding peptides. Nat. Rev. Bioeng. 2023;1:518–36.
[33] Glatter O, Kratky O. Small Angle X-ray Scattering. London: Academic; 1982.
[34] Feigin LA, Svergun DI. Structure Analysis by Small-Angle X-ray and Neutron Scattering. New York: Plenum; 1987.
[35] Roe R-J. Methods of X-ray and Neutron Scattering in Polymer Science. New York: Oxford University Press; 2000.
[36] Stribeck N. X-ray Scattering of Soft Matter. Berlin: Springer-Verlag; 2007.

[37] Svergun DI, Koch MHJ, Timmins PA, May RP. Small Angle X-ray and Neutron Scattering from Solutions of Biological Macromolecules. Oxford: Oxford University Press; 2013.
[38] de Jeu WH. Basic X-ray Scattering for Soft Matter. Oxford: Oxford University Press; 2016.
[39] Hamley IW. Small-Angle Scattering: Theory, Instrumentation, Data and Applications. Chichester: Wiley; 2021.
[40] Hashimoto T. Principles and Applications of X-ray, Light and Neutron Scattering. Singapore: Springer; 2022.
[41] Pedersen JS. Analysis of small-angle scattering data from colloids and polymer solutions: modeling and least-squares fitting. Adv. Colloid Interface Sci. 1997;70:171–210.
[42] Pedersen JS. Modelling of small-angle scattering data. In: Lindner P, Zemb T, editors. Neutrons, X-rays and Light. Scattering Methods Applied to Soft Condensed Matter. Amsterdam: Elsevier; 2002.
[43] Svergun DI, Koch MHJ. Small-angle scattering studies of biological macromolecules in solution. Rep. Prog. Phys. 2003;66(10):1735–82.
[44] Hamley IW, Castelletto V. Small-angle scattering of block copolymers in the melt, solution and crystal states. Prog. Polym. Sci. 2004;29:909–48.
[45] Putnam CD, Hammel M, Hura GL, Tainer JA. X-ray solution scattering (SAXS) combined with crystallography and computation: defining accurate macromolecular structures, conformations and assemblies in solution. Quart. Rev. Biophys. 2007;40(3):191–285.
[46] Narayanan T. High brilliance small-angle X-ray scattering applied to soft matter. Curr. Opin. Colloid Interface Sci. 2009;14(6):409–15.
[47] Jacques DA, Trewhella J. Small-angle scattering for structural biology-expanding the frontier while avoiding the pitfalls. Protein Sci. 2010;19(4):642–57.
[48] Rambo RP, Tainer JA. Super-resolution in solution X-ray scattering and its applications to structural systems biology. In: Dill KA, editor. Annual Review of Biophysics. Annual Reviews, 42; 2013. p. 415–41. Palo Alto.
[49] Pauw BR. Everything SAXS: small-angle scattering pattern collection and correction. J. Phys. Condens. Matter 2013;25(38):24.
[50] Vestergaard B. Analysis of biostructural changes, dynamics, and interactions - small-angle X-ray scattering to the rescue. Arch. Biochem. Biophys. 2016;602:69–79.
[51] Narayanan T, Wacklin H, Konovalov O, Lund R. Recent applications of synchrotron radiation and neutrons in the study of soft matter. Crystallogr. Rev 2017;23(3):160–226.
[52] Brosey CA, Tainer JA. Evolving SAXS versatility: solution X-ray scattering for macromolecular architecture, functional landscapes, and integrative structural biology. Curr. Opin. Struct. Biol. 2019;58:197–213.
[53] Qian S, Sharma VK, Clifton LA. Understanding the structure and dynamics of complex biomembrane interactions by neutron scattering techniques. Langmuir 2020;36(50):15189–211.
[54] Narayanan T, Konovalov O. Synchrotron scattering methods for nanomaterials and soft matter research. Materials 2020;13(3).
[55] Jeffries CM, Ilavsky J, Martel A, Hinrichs S, Meyer A, Pedersen JS, et al. Small-angle X-ray and neutron scattering. Nat. Rev. Methods Primers 2021;1(1).
[56] Ochbaum G, Bitton R. Using small-angle X-ray scattering (SAXS) to study the structure of self-assembling biomaterials. In: Azevedo HS, Da Silva RMP, editors. Self-Assembling Biomaterials: Molecular Design, Characterization and Application in Biology and Medicine; 2018. p. 291–304.
[57] McDowall D, Adams DJ, Seddon AM. Using small angle scattering to understand low molecular weight gels. Soft Matter 2022;18(8):1577–90.
[58] Hamley IW, Castelletto V, Dehsorkhi A, Torras J, Aleman C, Portnaya I, et al. The conformation and aggregation of proline-rich surfactant-like peptides. J. Phys. Chem. B 2018;122(6):1826–35.
[59] Castelletto V, Barnes RH, Karatzas KA, Edwards-Gayle CJC, Greco F, Hamley IW, et al. Arginine-containing surfactant-like peptides: interaction with lipid membranes and antimicrobial activity. Biomacromolecules 2018;19:2782–7294.
[60] Hamley IW, Dehsorkhi A, Castelletto V, Walter MNM, Connon CJ, Reza M, et al. Self-Assembly and Collagen Stimulating Activity of a Peptide Amphiphile Incorporating a Peptide Sequence from Lumican. Langmuir 2015;31:4490–5.
[61] Hamley IW, Dehsorkhi A, Castelletto V, Furzeland S, Atkins D, Seitsonen J, et al. Reversible helical ribbon unwinding transition of a self-assembling peptide amphiphile. Soft Matter 2013;9:9290–3.
[62] Hamley IW, Castelletto V. Characterization of peptides and their assemblies. In: Guler MO, editor. Peptide-Based Biomaterials. Cambridge: Royal Society of Chemistry; 2021.
[63] Dehsorkhi A, Hamley IW, Seitsonen J, Ruokolainen J. Tuning self-assembled nanostructures through enzymatic degradation of a peptide amphiphile. Langmuir 2013;29:6665–72.
[64] Hamley IW, Dehsorkhi A, Jauregi P, Seitsonen J, Ruokolainen J, Coutte F, et al. Self-assembly of three bacterially-derived bioactive lipopeptides. Soft Matter 2013;9:9572–8.
[65] Miravet JF, Escuder B, Segarra-Maset MD, Tena-Solsona M, Hamley IW, Dehsorkhi A, et al. Self-assembly of a peptide amphiphile: transition from nanotape fibrils to micelles. Soft Matter 2013;9:3558–64.
[66] Hamley IW, Kirkham S, Dehsorkhi A, Castelletto V, Reza M, Ruokolainen J. Toll-like receptor agonist lipopeptides self-assemble into distinct nanostructures. Chem. Commun. 2014;50:15948–51.
[67] Dehsorkhi A, Gouveia RJ, Smith AM, Hamley IW, Castelletto V, Connon CJ, et al. Self-assembly of a dual functional bioactive peptide amphiphile incorporating both matrix metalloprotease substrate and cell adhesion motifs. Soft Matter 2015;11:3115–24.
[68] Hutchinson JA, Burholt S, Hamley IW, Lundback A-K, Uddin S, dos Santos AG, et al. The effect of lipidation on the self-assembly of the gut derived peptide hormone PYY3-36. Bioconj. Chem. 2018;29:2296–308.
[69] Castelletto V, Hamley IW, Seitsonen J, Ruokolainen J, Harris G, Bellmann-Sickert K, et al. Conformation and aggregation of selectively PEGylated and lipidated gastric peptide hormone human PYY_{3-36}. Biomacromolecules 2018;19(11):4320–32.
[70] Castelletto V, McKendrick JME, Hamley IW, Cenker C, Olsson U. PEGylated amyloid peptide nanocontainer delivery and release system. Langmuir 2010;26:11624–7.
[71] Shi YJ, Hu Y, Ochbaum G, Lin R, Bitton R, Cui HG, et al. Enzymatic activation of cell-penetrating peptides in self-assembled nanostructures triggers fibre-to-micelle morphological transition. Chem. Commun. 2017;53(52):7037–40.
[72] Hamley IW, Krysmann MJ, Castelletto V, Kelarakis A, Noirez L, Hule RA, et al. Nematic and columnar ordering of a PEG-peptide conjugate in aqueous solution. Chem. Eur. J. 2008;14:11369–74.
[73] Hamley IW, Krysmann MJ, Castelletto V, Noirez L. Multiple lyotropic polymorphism of a PEG-peptide diblock copolymer in aqueous solution. Adv. Mater. 2008;20:4394–7.
[74] Thiyagarajan P, Burkoth TS, Urban V, Seifert S, Benzinger TLS, Morgan DM, et al. pH dependent self assembly of β-amyloid(10-35) and β-amyloid(10-35)-PEG3000. J. Appl. Crystallogr. 2000;33:535–9.
[75] Draper ER, Dietrich B, McAulay K, Brasnett C, Abdizadeh H, Patmanidis I, et al. Using small-angle scattering and contrast matching to understand molecular packing in low molecular weight gels. Matter 2020;2(3):764–78.
[76] Pabst G, Rappolt M, Amenitsch H, Laggner P. Structural information from multilamellar liposomes at full hydration: full q-range fitting with high quality X-ray data. Phys. Rev. E 2000;62(3):4000–9.
[77] Castelletto V, Cheng G, Stain C, Connon CJ, Hamley IW. Self-assembly of a peptide amphiphile containing L-carnosine and its mixtures with a multilamellar vesicle forming lipid. Langmuir 2012;28(31):11599–608.
[78] Hamley IW, Dehsorkhi A, Castelletto V. Self-assembled arginine-coated peptide nanosheets in water. Chem. Commun. 2013;49:1850–2.
[79] Castelletto V, Gouveia RJ, Connon CJ, Hamley IW. New RGD- peptide amphiphile mixtures containing a negatively charged diluent. Farad. Discuss. 2013;166:381–97.
[80] Castelletto V, Edwards-Gayle CJC, Greco F, Hamley IW, Seitsonen J, Ruokolainen J. Self-assembly, tunable hydrogel properties and selective anti-cancer activity of a carnosine-derived lipidated peptide. ACS Appl. Mater. Interfaces 2019;11:33573–80.
[81] Castelletto V, Hamley IW. Amyloid and hydrogel formation of a peptide sequence from a coronavirus spike protein. ACS Nano 2022;16:1857–67.
[82] Edwards-Gayle CJC, Barrett G, Roy S, Castelletto V, Seitsonen J, Ruokolainen J, et al. Selective antibacterial activity and lipid membrane interactions of arginine-rich amphiphilic peptides. ACS Appl. Bio. Mater. 2020;3:1165–75.
[83] Rosa E, de Mello L, Castelletto V, Dallas ML, Accardo A, Seitsonen J, et al. Cell adhesion motif-functionalized lipopeptides: nanostructure and selective myoblast cytocompatibility. Biomacromolecules 2023;24(213-224).
[84] Moyer TJ, Cui H, Stupp SI. Tuning nanostructure dimensions with supramolecular twisting. J. Phys. Chem. B 2012;117:4604–10.
[85] Pringle OA, Schmidt PW. Small-angle x-ray scattering from helical macromolecules. J. Appl. Crystallogr. 1971;4:290–3.
[86] Hamley IW. Form factor of helical ribbons. Macromolecules 2008;41:8948–50.
[87] Teixeira CV, Amenitsch H, Fukushima T, Hill JP, Jin W, Aida T, et al. Form factor of an N-layered helical tape and its application to nanotube formation of hexa-peri-hexabenzocoronene-based molecules. J. Appl. Crystallogr. 2010;43:850–7.
[88] Terech P, Velu SKP, Pernot P, Wiegart L. Salt effects in the formation of self-assembled lithocholate helical ribbons and tubes. J. Phys. Chem. B 2012;116(36):11344–55.
[89] McCourt JM, Kewalramani S, Gao C, Roth EW, Weigand SJ, Olvera de la Cruz M, et al. Electrostatic control of shape selection and nanoscale structure in chiral molecular assemblies. ACS Central Sci. 2022;8:1169–81.
[90] Lu K, Jacob J, Thiyagarajan P, Conticello VP, Lynn DG. Exploiting amyloid fibril lamination for nanotube self assembly. J. Am. Chem. Soc. 2003;125:6391–3.
[91] Hamley IW, Burholt S, Hutchinson J, Castelletto V, da Silva ER, Alves WA, et al. Shear alignment of bola-amphiphilic arginine-coated peptide nanotubes. Biomacromolecules 2017;18:141–9.
[92] Bucak S, Cenker C, Nasir I, Olsson U, Zackrisson M. Peptide nanotube nematic phase. Langmuir 2009;25(8):4262–5.
[93] Rüter A, Kuczera S, Stenhammar J, Zinn T, Narayanan T, Olsson U. Tube to ribbon transition in a self-assembling model peptide system. Phys. Chem. Chem. Phys. 2020;22(33):18320–7.
[94] Valery C, Paternostre M, Robert B, Gulik-Krzywicki T, Narayanan T, Dedieu JC, et al. Biomimetic organization: Octapeptide self-assembly into nanotubes of viral capsid-like dimension. Proc. Natl. Acad. Sci. USA 2003;100(18):10258–62.
[95] Valéry C, et al. Self-association process of a peptide in solution: from b-sheet filaments to large embedded nanotubes. Biophys. J. 2004;86:2484–501.
[96] Pouget E, Fay N, Dujardin E, Jamin N, Berthault P, Perrin L, et al. Elucidation of the self-assembly pathway of lanreotide octapeptide into beta-sheet nanotubes: role of two stable intermediates. J. Am. Chem. Soc. 2010;132(12):4230–41.
[97] Tarabout C, Roux S, Gobeaux F, Fay N, Pouget E, Meriadec C, et al. Control of peptide nanotube diameter by chemical modifications of an aromatic residue involved in a single close contact. Proc. Natl. Acad. Sci. USA 2011;108(19):7679–84.

[98] Gobeaux F, Fay N, Tarabout C, Meriadec C, Meneau F, Ligeti M, et al. Structural role of counterions adsorbed on self-assembled peptide nanotubes. J. Am. Chem. Soc. 2012;134(1):723–33.
[99] Gobeaux F, Fay N, Tarabout C, Meneau F, Meriadec C, Delvaux C, et al. Experimental observation of double-walled peptide nanotubes and monodispersity modeling of the number of walls. Langmuir 2013;29(8):2739–45.
[100] Pouget E, Dujardin E, Cavalier A, Moreac A, Valery C, Marchi-Artzner V, et al. Hierarchical architectures by synergy between dynamical template self-assembly and biomineralization. Nat. Mater. 2007;6(6):434–9.
[101] Zhao YR, Deng L, Wang JQ, Xu H, Lu JR. Solvent controlled structural transition of Kl(4)K self-assemblies: from nanotubes to nanofibrils. Langmuir 2015;31(47):12975–83.
[102] Valéry C, Artzner F, Paternostre M. Peptide nanotubes: molecular organisations, self-assembly mechanisms and applications. Soft Matter 2011;7:9583–94.
[103] Mello LR, Aguiar RB, Yamada RY, Moraes JZ, Hamley IW, Alves WA, et al. Amphipathic design dictates self-assembly, cytotoxicity and cell uptake of arginine-rich surfactant-like peptides. J. Mater. Chem. B 2020;8(12):2495–507.
[104] Pelin JNBD, Gerbelli BB, Edwards-Gayle CJC, Aguilar AM, Castelletto V, Hamley IW, et al. Amyloid peptide mixtures: self-assembly, hydrogelation, nematic ordering, and catalysts in aldol reactions. Langmuir 2020;36(11):2767–74.
[105] Fisher ME, Burford RJ. Theory of critical-point scattering and correlations. I. The Ising model. Phys. Rev. 1967;126(2):583–622.
[106] de Mello LR, Castelletto V, Hamley IW, Garcia BBM, Han SW, de Oliveira CLP, et al. Nanoscopic structure of complexes formed between DNA and the cell-penetrating peptide penetratin. J. Phys. Chem. B. 2019;123(42):8861–71.
[107] Silva ER, Listik E, Han SW, Alves WA, Soares BM, Reza M, et al. Sequence length dependence in arginine/phenylalanine oligopeptides: implications for self-assembly and cytotoxicity. Biophys. Chem. 2018;233:1–12.
[108] Teixeira J. Small-angle scattering by fractal systems. J. Appl. Crystallogr. 1988;21:781–5.
[109] Beaucage G. Approximations leading to a unified exponential power-law approach to small-angle scattering. J. Appl. Crystallogr. 1995;28:717–28.
[110] Beaucage G. Small-angle scattering from polymeric mass fractals of arbitrary mass-fractal dimension. J. Appl. Crystallogr. 1996;29:134–46.
[111] Mello LR, Hamley IW, Miranda A, Alves WA, Silva ER. β-sheet assembly in amyloidogenic glutamic acid nanostructures: insights from X-ray scattering and infrared nanospectroscopy. J. Pept. Sci. 2019;25(6):12.
[112] Mello LR, Hamley IW, Castelletto V, Garcia BBM, Lourenco TC, Vassiliades SV, et al. Self-assembly and intracellular delivery of DNA by a truncated fragment derived from the Trojan peptide Penetratin. Soft Matter 2020;16(20):4746–55.
[113] Maslovskis A, Guilbaud JB, Grillo I, Hodson N, Miller AF, Saiani A. Self-assembling peptide/thermoresponsive polymer composite hydrogels: effect of peptide-polymer interactions on hydrogel properties. Langmuir 2014;30(34):10471–80.
[114] Chapman R, Koh ML, Warr GG, Jolliffe KA, Perrier S. Structure elucidation and control of cyclic peptide-derived nanotube assemblies in solution. Chem. Sci. 2013;4(6):2581–9.
[115] Haertlein M, Moulin M, Devos JM, Laux V, Dunne O, Forsyth VT. Biomolecular deuteration for neutron structural biology and dynamics. In: Kelman Z, editor. Isotope Labeling of Biomolecules – Applications; 2016. p. 113–57.
[116] Gerbelli BB, Perdo LO, Cortez B, Sodre PT, Coutinho MD, Hamley IW, et al. Interaction between glyphosate pesticide and amphiphilic peptides for colorimetric analysis. Nanoscale Adv. 2022;4(17):3592–9.
[117] Cui HG, Cheetham AG, Pashuck ET, Stupp SI. Amino acid sequence in constitutionally isomeric tetrapeptide amphiphiles dictates architecture of one-dimensional nanostructures. J. Am. Chem. Soc. 2014;136(35):12461–8.
[118] Kohlbrecher J. https://sasfit.org/; accessed in 2023.
[119] SASView, http://www.sasview.org/; accessed in 2023.
[120] Spinozzi F, Ferrero C, Ortore MG, Antolinos AD, Mariani P. GENFIT: software for the analysis of small-angle X-ray and neutron scattering data of macromolecules in solution. J. Appl. Crystallogr. 2014;47:1132–9.
[121] Heenan R. FISH. 2018.
[122] Svergun D, Barberato C, Koch MHJ. CRYSOL - a program to evaluate x-ray solution scattering of biological macromolecules from atomic coordinates. J. Appl. Crystallogr. 1995;28:768–73.
[123] Franke D, Petoukhov MV, Konarev PV, Panjkovich A, Tuukkanen A, Mertens HDT, et al. ATSAS 2.8: a comprehensive data analysis suite for small-angle scattering from macromolecular solutions. J. Appl. Crystallogr. 2017;50:1212–25.
[124] Schneidman-Duhovny D, Hammel M, Tainer JA, Sali A. Accurate SAXS profile computation and its assessment by contrast variation experiments. Biophys. J. 2013;105(4):962–74.
[125] Schneidman-Duhovny D, Hammel M, Tainer JA, Sali A. FoXS, FoXSDock and MultiFoXS: single-state and multi-state structural modeling of proteins and their complexes based on SAXS profiles. Nucleic Acids Res. 2016;44(W1):W424–9.
[126] Putnam DK, Lowe EW, Meiler J. Reconstruction of SAXS profiles from protein structures. Comput. Struct. Biotech. J. 2013;8(11):e201308006.
[127] Hamley IW. Introduction to Soft Matter. Revised ed. Chichester: Wiley; 2007.
[128] Jacoby G, Asher MS, Ehm T, Ionita IA, Shinar H, Azoulay-Ginsburg S, et al. Order from disorder with intrinsically disordered peptide amphiphiles. J. Am. Chem. Soc. 2021;143(30):11879–88.
[129] Ehm T, Shinar H, Jacoby G, Meir S, Koren G, Asher MS, et al. Self-assembly of tunable intrinsically disordered peptide amphiphiles. Biomacromolecules 2023;24:98–108.
[130] Hule RA, Nagarkar RP, Altunbas A, Ramay HR, Branco MC, Schneider JP, et al. Correlations between structure, material properties and bioproperties in self-assembled beta-hairpin peptide hydrogels. Farad. Discuss. 2008;139:251–64.
[131] Pedersen JS, Schurtenberger P. Scattering functions of semi-flexible polymers with and without excluded volume effects. Macromolecules 1996;29(23):7602–12.
[132] Castelletto V, de Mello LR, Arfara F, Iatrou H, Seitsonen J, Hamley IW. Influence of polymer molar mass and mixture stoichiometry on polyelectrolyte complexes of poly(L-arginine) and poly(L-glutamic acid). Polymer 2022;263:125497.
[133] Marciel AB, Srivastava S, Tirrell MV. Structure and rheology of polyelectrolyte complex coacervates. Soft Matter 2018;14(13):2454–64.
[134] de Mello LR, Carrascosa V, Rebelato E, Juliano MA, Hamley IW, Castelletto V, et al. Nanostructure formation and cell spheroid morphogenesis of a peptide supramolecular hydrogel. Langmuir 2022;38(11):3434–45.
[135] Gayen K, Nandi N, Das KS, Hermida-Merino D, Hamley IW, Banerjee A. The aging effect on the enhancement of thermal stability, mechanical stiffness and fluorescence properties of histidine-appended naphthalenediimide based two-component hydrogels. Soft Matter 2020;16(44):10106–14.
[136] Hamley IW, Cheng G, Castelletto V. Self-assembly of telechelic PEG end-capped with hydrophobic dipeptides. Macromol. Biosci. 2011;11:1068–78.
[137] Mondal B, Gupta VK, Hansda B, Bhoumik A, Mondal T, Majumder HK, et al. Amino acid containing amphiphilic hydrogelators with antibacterial and antiparasitic activities. Soft Matter 2022;18(37):7201–16.
[138] Gayen K, Basu K, Bairagi D, Castelletto V, Hamley IW, Banerjee A. Amino-acid-based metallo-hydrogel that acts like an esterase. ACS Appl. Bio. Mater. 2018;1(5):1717–24.
[139] Bairagi D, Biswas P, Basu K, Hazra S, Hermida-Merino D, Sinha DK, et al. Self-assembling peptide-based hydrogel: regulation of mechanical stiffness and thermal stability and 3D cell culture of fibroblasts. ACS Appl. Bio. Mater. 2019;2(12):5235–44.
[140] Castelletto V, Hamley IW, Perez J, Abezgauz L, Danino D. Fibrillar superstructure from extended nanotapes formed by a collagen-stimulating peptide. Chem. Commun. 2010;46:9185–7.
[141] Dehsorkhi A, Castelletto V, Hamley IW, Adamcik J, Mezzenga R. The effect of pH on the self-assembly of a collagen derived peptide amphiphile. Soft Matter 2013;9:6033–6.
[142] Castelletto V, Hamley IW, Whitehouse C, Matts P, Osborne R, Baker ES. Self-assembly of palmitoyl lipopeptides used in skin care products. Langmuir 2013;29:9149–55.
[143] Gerbelli BB, Oliveira CLP, Silva ER, Hamley IW, Alves WA. Amyloid formation by short peptides in the presence of dipalmitoylphosphatidylcholine membranes. Langmuir 2020;36(48):14793–801.
[144] Dehsorkhi A, Castelletto V, Hamley IW, Seitsonen J, Ruokolainen J. Interaction between a cationic surfactant-like peptide and lipid vesicles and its relationship to antimicrobial activity. Langmuir 2013;29:14246–53.
[145] Castelletto V, Edwards-Gayle CJC, Hamley IW, Barrett G, Seitsonen J, Ruokolainen J. Peptide-stabilized emulsions and gels from an arginine-rich surfactant-like peptide with antimicrobial activity. ACS Appl. Mater. Interfaces 2019;11(10):9893–903.
[146] Castelletto V, Barnes RH, Karatsas K-A, Edwards-Gayle CJC, Greco F, Hamley IW, et al. Restructuring of lipid membranes by an arginine-capped peptide bolaamphiphile. Langmuir 2019;35:1302–11.
[147] Edwards-Gayle CJC, Castelletto V, Hamley IW, Barrett G, Greco F, Hermida-Merino D, et al. Self-assembly, antimicrobial activity and membrane interactions of arginine-capped peptide bola-amphiphiles. ACS Appl. Bio. Mater. 2019;2:2208–18.
[148] Mishra A, Lai GH, Schmidt NW, Sun VZ, Rodriguez AR, Tong R, et al. Translocation of HIV TAT peptide and analogues induced by multiplexed membrane and cytoskeletal interactions. Proc. Natl. Acad. Sci. USA 2011;108(41):16883–8.
[149] Nielsen JE, Prevost SF, Jenssen H, Lund R. Impact of antimicrobial peptides on E. coli-mimicking lipid model membranes: correlating structural and dynamic effects using scattering methods. Farad. Discuss. 2021;232:203–17.
[150] Nielsen JE, Lund R. Molecular transport and growth of lipid vesicles exposed to antimicrobial peptides. Langmuir 2022;38(1):374–84.
[151] Nielsen JE, Bjornestad VA, Lund R. Resolving the structural interactions between antimicrobial peptides and lipid membranes using small-angle scattering methods: the case of indolicidin. Soft Matter 2018;14(43):8750–63.
[152] Preu J, Jaeger T, Garamus VM, Gutberlet T. Use of small angle neutron scattering to study the interaction of angiotensin II with model membranes. Eur. Biophys. J. Biophys. Lett. 2011;40(5):687–98.
[153] Mishra A, Gordon VD, Yang LH, Coridan R, Wong GCL. HIV TAT forms pores in membranes by inducing saddle-splay curvature: potential role of bidentate hydrogen bonding. Angew. Chem., Int. Ed. Engl. 2008;47(16):2986–9.
[154] Schmidt N, Mishra A, Lai GH, Wong GCL. Arginine-rich cell-penetrating peptides. FEBS Lett. 2009;584:1806–13.
[155] Lee EY, Fulan BM, Wong GCL, Ferguson AL. Mapping membrane activity in undiscovered peptide sequence space using machine learning. Proc. Natl. Acad. Sci. USA 2016;113(48):13588–93.
[156] Bitton R, Chow LW, Zha RH, Velichko YS, Pashuck ET, Stupp SI. Electrostatic control of structure in self-assembled membranes. Small 2014;10(3):500–5.
[157] Matson JB, Navon Y, Bitton R, Stupp SI. Light-controlled hierarchical self-assembly of polyelectrolytes and supramolecular polymers. ACS Macro Lett. 2015;4(1):43–7.

[158] Inostroza-Brito KE, Collin E, Siton-Mendelson O, Smith KH, Monge-Marcet A, Ferreira DS, et al. Co-assembly, spatiotemporal control and morphogenesis of a hybrid protein-peptide system. Nat. Chem. 2015;7(11):897–904.
[159] Yosefi G, Levi T, Rapaport H, Bitton R. Time matters for macroscopic membranes formed by alginate and cationic beta-sheet peptides. Soft Matter 2020;16(44): 10132–42.
[160] Yosefi G, Cohen-Erez I, Nativ-Roth E, Rapaport H, Bitton R. Spontaneous alignment of self-assembled cationic and amphiphilic beta-sheet peptides. Adv. Mater. Interf. 2020;7(14).
[161] Ochbaum G, Davidovich-Pinhas M, Bitton R. Tuning the mechanical properties of alginate-peptide hydrogels. Soft Matter 2018;14(21):4364–73.
[162] Radvar E, Shi YJ, Grasso S, Edwards-Gayle CJC, Liu XT, Mauter MS, et al. Magnetic field-induced alignment of nanofibrous supramolecular membranes: a molecular design approach to create tissue-like biomaterials. ACS Appl. Mater. Interfaces 2020;12(20):22661–72.
[163] Zhang SM, Greenfield MA, Mata A, Palmer LC, Bitton R, Mantei JR, et al. A self-assembly pathway to aligned monodomain gels. Nat. Mater. 2010;9(7):594–601.
[164] Manalastas-Cantos K, Konarev PV, Hajizadeh NR, Kikhney AG, Petoukhov MV, Molodenskiy DS, et al. ATSAS 3.0: expanded functionality and new tools for small-angle scattering data analysis. J. Appl. Crystallogr. 2021;54:343–55.
[165] Petoukhov MV, Franke D, Shkumatov AV, Tria G, Kikhney AG, Gajda M, et al. New developments in the ATSAS program package for small-angle scattering data analysis. J. Appl. Crystallogr. 2012;45:342–50.
[166] Vestergaard B, Groenning M, Roessle M, Kastrup JS, van de Weert M, Flink JM, et al. A helical structural nucleus is the primary elongating unit of insulin amyloid fibrils. PLoS Biol. 2007;5(5):1089–97.
[167] Oliveira CLP, Behrens MA, Pedersen JS, Erlacher K, Otzen D, Pedersen JS. A SAXS study of glucagon fibrillation. J. Mol. Biol. 2009;387(1):147–61.
[168] Giehm L, Svergun DI, Otzen DE, Vestergaard B. Low-resolution structure of a vesicle disrupting alpha-synuclein oligomer that accumulates during fibrillation. Proc. Natl. Acad. Sci. USA 2011;108(8):3246–51.
[169] Langkilde AE, Morris KL, Serpell LC, Svergun DI, Vestergaard B. The architecture of amyloid-like peptide fibrils revealed by X-ray scattering, diffraction and electron microscopy. Acta Crystallogr. Sect. D-Struct. Biol. 2015;71:882–95.
[170] Glatter O. A new method for the evaluation of small-angle scattering data. J. Appl. Crystallogr. 1977;10:415–21.
[171] Hutchinson JA, Hamley IW, Torras J, Aleman C, Seitsonen J, Ruokolainen J. Self-assembly of lipopeptides containing short peptide fragments derived from the gastrointestinal hormone PYY3−36: from micelles to amyloid fibrils. J. Phys. Chem. B 2019;123:614–21.
[172] Castelletto V, Kaur A, Hamley IW, Barnes RH, Karatzas KA, Hermida-Merino D, et al. Hybrid membrane biomaterials from self-assembly in polysaccharide and peptide amphiphile mixtures: controllable structural and mechanical properties and antimicrobial activity. RSC Adv. 2017;7(14):8366–75.
[173] Tiggelaar SM, Mossou E, Callow P, Callow S, Teixeira SCM, Mitchell EP, et al. Neutron fibre diffraction studies of amyloid using H2O/D2O isotopic replacement. Acta Crystallogr. F-Struct. Biol. Commun. 2011;67:332–5.
[174] Narayanan T, Ruter A, Olsson U. Multiscale structural elucidation of peptide nanotubes by X-ray scattering methods. Front. Bioeng. Biotech. 2021;9.
[175] Castelletto V, Seitsonen J, Ruokolainen J, Hamley IW. Alpha helical surfactant-like peptides self-assemble into pH-dependent nanostructures. Soft Matter 2020; 17:3096–104.
[176] Hamley IW, Dehsorkhi A, Castelletto V. Coassembly in binary mixtures of peptide amphiphiles containing oppositely charged residues. Langmuir 2013;29:5050–9.
[177] Ali HAA, Griveau A, Artzner F, Dupont A, Lautram N, Jourdain MA, et al. Investigation on the self-assembly of the NFL-TBS.40-63 peptide and its interaction with gold nanoparticles as a delivery agent for glioblastoma. Int. J. Pharm. X 2022;4.
[178] Chervy P, Petcut C, Rault D, Meriadec C, Bizien T, Francois K, et al. Organic nanoscrolls from electrostatic interactions between peptides and lipids: assembly steps and structure. Langmuir 2019;35(32):10648–57.
[179] Qiu RM, Sasselli IR, Alvarez Z, Sai H, Ji W, Palmer LC, et al. Supramolecular copolymers of peptides and lipidated peptides and their therapeutic potential. J. Am. Chem. Soc. 2022;144(12):5562–74.
[180] Yuan SC, Lewis JA, Sai H, Weigand SJ, Palmer LC, Stupp SI. Peptide sequence determines structural sensitivity to supramolecular polymerization pathways and bioactivity. J. Am. Chem. Soc. 2022;144(36):16512–23.
[181] Wester JR, Lewis JA, Freeman R, Sai H, Palmer LC, Henrich SE, et al. Supramolecular exchange among assemblies of opposite charge leads to hierarchical structures. J. Am. Chem. Soc. 2020;142(28):12216–25.
[182] Cui HG, Pashuck ET, Velichko YS, Weigand SJ, Cheetham AG, Newcomb CJ, et al. Spontaneous and X-ray-triggered crystallization at long range in self-assembling filament networks. Science 2010;327(5965):555–9.
[183] Krysmann MJ, Funari SS, Canetta E, I.W.. Hamley the effect of PEG crystallization on the morphology of PEG-peptide block copolymers containing amyloid β peptide fragments. Macromol. Chem. Phys. 2008;209:883–9.
[184] Hamley IW, Krysmann MJ. Effect of PEG crystallization on the self-assembly of PEG/peptide copolymers containing amyloid peptide fragments. Langmuir 2008; 24:8210–4.
[185] Diaferia C, Sibillano T, Altamura D, Roviello V, Vitagliano L, Giannini C, et al. Structural characterization of PEGylated hexaphenylalanine nanostructures exhibiting green photoluminescence emission. Chem. Eur. J. 2017;23(56): 14039–48.
[186] Kirby NM, Cowieson NP. Time-resolved studies of dynamic biomolecules using small angle X-ray scattering. Curr. Opin. Struct. Biol. 2014;28:41–6.
[187] Levantino M, Yorke BA, Monteiro DCF, Cammarata M, Pearson AR. Using synchrotrons and XFELs for time-resolved X-ray crystallography and solution scattering experiments on biomolecules. Curr. Opin. Struct. Biol. 2015;35:41–8.
[188] Tuukkanen AT, Spilotros A, Svergun DI. Progress in small-angle scattering from biological solutions at high-brilliance synchrotrons. IUCrJ 2017;4:518–28.
[189] Trewhella J. Recent advances in small-angle scattering and its expanding impact in structural biology. Structure 2022;30(1):15–23.
[190] Levantino M, Schiro G, Lemke HT, Cottone G, Glownia JM, Zhu DL, et al. Ultrafast myoglobin structural dynamics observed with an X-ray free-electron laser. Nat. Commun. 2015;6:6.
[191] Bernado P, Mylonas E, Petoukhov MV, Blackledge M, Svergun DI. Structural characterization of flexible proteins using small-angle X-ray scattering. J. Am. Chem. Soc. 2007;129(17):5656–64.
[192] Pelikan M, Hura GL, Hammel M. Structure and flexibility within proteins as identified through small angle X-ray scattering. Gen. Physiol. Biophys. 2009;28 (2):174–89.
[193] Krukenberg KA, Street TO, Lavery LA, Agard DA. Conformational dynamics of the molecular chaperone Hsp90. Quart. Rev. Biophys. 2011;44(2):229–55.
[194] Cho HS, Schotte F, Dashdorj N, Kyndt J, Henning R, Anfinrud PA. Picosecond photobiology: watching a signaling protein function in real time via time-resolved small- and wide-angle X-ray scattering. J. Am. Chem. Soc. 2016;138(28): 8815–23.
[195] Lorenzen N, Nielsen SB, Buell AK, Kaspersen JD, Arosio P, Vad BS, et al. The role of stable alpha-synuclein oligomers in the molecular events underlying amyloid formation. J. Am. Chem. Soc. 2014;136(10):3859–68.
[196] Ortony JH, Newcomb CJ, Matson JB, Palmer LC, Doan PE, Hoffman BM, et al. Internal dynamics of a supramolecular nanofibre. Nat. Mater. 2014;13(8):812–6.
[197] Ortony JH, Qiao BF, Newcomb CJ, Keller TJ, Palmer LC, Deiss-Yehiely E, et al. Water dynamics from the surface to the interior of a supramolecular nanostructure. J. Am. Chem. Soc. 2017;139(26):8915–21.
[198] Lund R, Willner L, Richter D, Dormidontova EE. Equilibrium chain exchange kinetics of diblock copolymer micelles: tuning and logarithmic relaxation. Macromolecules 2006;39(13):4566–75.
[199] Hollamby MJ. Practical applications of small-angle neutron scattering. Phys. Chem. Chem. Phys. 2013;15(26):10566–79.
[200] Lund R, Willner L, Richter D. Kinetics of block copolymer micelles studied by small-angle scattering methods. In: Abe A, Lee KS, Leibler L, Kobayashi S, editors. Controlled Polymerization and Polymeric Structures: Flow Microreactor Polymerization, Micelles Kinetics, Polypeptide Ordering, Light Emitting Nanostructures. Berlin: Springer-Verlag Berlin; 2013. p. 51–158.
[201] Lu J, Bates FS, Lodge TP. Remarkable effect of molecular architecture on chain exchange in triblock copolymer micelles. Macromolecules 2015;48(8):2667–76.
[202] Pabit SA, Meisburger SP, Li L, Blose JM, Jones CD, Pollack L. Counting ions around DNA with anomalous small-angle X-ray scattering. J. Am. Chem. Soc. 2010;132(46):16334–6.
[203] Pollack L. SAXS studies of ion-nucleic acid interactions. In: Rees DC, Dill KA, Williamson JR, editors. Annual Review of Biophysics. Vol 40; 2011. p. 225–42.
[204] Guilleaume B, Ballauf M, Goegrik G, Wittemann M, Rehahn M. Correlation of counterions with rodlike macroions as assessed by anomalous small-angle X-ray scattering. Colloid Polym. Sci. 2001;279:829–35.
[205] Riekel C, Burghammer M, Muller M. Microbeam small-angle scattering experiments and their combination with microdiffraction. J. Appl. Crystallogr. 2000;33(1):421–3.
[206] Riekel C. Applications of micro-SAXS/WAXS to study polymer fibers. In: Nuclear Instruments & Methods in Physics Research Section B-Beam Interactions with Materials and Atoms. 199; 2003. p. 106–11.
[207] Grage SL, Afonin S, Kara S, Buth G, Ulrich AS. Membrane thinning and thickening induced by membrane-active amphipathic peptides. Front. Cell Dev. Biol. 2016;4.
[208] Zabara M, Ren Q, Amenitsch H, Salentinig S. Bioinspired antimicrobial coatings from peptide-functionalized liquid crystalline nanostructures. ACS Appl. Bio. Mater. 2021;4(6):5295–303.
[209] Franke D, Jeffries CM, Svergun DI. Machine learning methods for X-ray scattering data analysis from biomacromolecular solutions. Biophys. J. 2018;114(11): 2485–92.
[210] Chen YL, Pollack L. Machine learning deciphers structural features of RNA duplexes measured with solution X-ray scattering. IUCrJ 2020;7:870–80.
[211] Bras W, Koizumi S, Terrill NJ. Beyond simple small-angle X-ray scattering: developments in online complementary techniques and sample environments. IUCrJ 2014;1:478–91.